Srivastava, A. and Needleman, A., 2025. Non-Schmid continuum slip crystal plasticity with implications for dissipation rate. Journal of the Mechanics and Physics of Solids, 194, p.105928.

Non-Schmid Continuum Slip Crystal Plasticity with Implications for Dissipation Rate

Ankit Srivastava, Alan Needleman

Department of Materials Science & Engineering, Texas A&M University, College Station, TX 77843 USA

Abstract

Finite deformation finite element calculations are carried out to analyze nonuniform plane strain tensile deformation of single crystals using an elastic-viscoplastic crystal plasticity constitutive relation. The planar crystals considered have two potentially active slip systems with the driving force for slip including a non-Schmid stress. The non-Schmid stress on a slip system is taken to be dependent on the Schmid resolved shear stress on the other slip system. In the calculations, the parameters characterizing the non-Schmid term, including its magnitude and the slip interval over which it acts, are varied. The effects of non-Schmid governed slip on the overall stress-strain response and on the strain at which a rapid drop in overall stress occurs is investigated. Additionally, the dissipation rate associated with non-Schmid governed slip is calculated both pointwise and integrated over the entire domain. Results show that one consequence of non-Schmid governed slip is the change in the slip mode and another consequence is that a non-negative dissipation rate for all possible deformation histories is not guaranteed. However, stable calculations up to the rapid drop in overall stress can be carried out even with the dissipation rate being negative at one or more points in the domain over some strain range and, in some cases, even when the integrated dissipation rate is negative. Implications for possible constitutive restrictions are briefly considered.

Keywords: Crystal Plasticity, Dissipation Rate, Non-Schmid Governed Slip, Slip Mode, Localization

---

1. Introduction

Within the context of continuum slip crystal plasticity, Schmid's law states that the slip rate on a slip system (a combination of slip direction and slip plane normal) is governed by the resolved shear stress on that system. As noted by Vitek et al. (2004); Vitek and Paidar (2008), for plastic deformation by dislocation glide, Schmid's law generally holds for fcc crystals and to an extent for hcp crystals when dislocation glide is restricted to basal planes. However, even for fcc crystals, when cross-slip occurs, stresses other than the Schmid resolved shear stress can play a significant role, see Hussein et al. (2015); Malka-Markovitz et al. (2021).

Deviations from Schmid's law have also been observed for a wide variety of crystalline solids including intermetallics (Ghorbanpour et al., 2020, 2017; Gröger, 2021; Qin and Bassani, 1992), such as Ni_3Al, Ni_2Ga, and Co_3Ti; MAX phases (Zhan et al., 2020, 2021); and bcc crystals, such as α-iron (Chen et al., 2014; Koester et al., 2012; Lim et al., 2015; Patra et al., 2014; Srivastava et al., 2015), molybdenum and tungsten (Cereceda et al., 2016; Gröger et al., 2008a,b), chromium (Gröger and Vitek, 2020), and tantalum–tungsten alloys (Knezevic et al., 2014).

Within the context of discrete dislocation plasticity, formulations involving non-Schmid stress dependence have been developed, e.g., Chaussidon et al. (2008); Wang and Beyerlein (2011). Indeed, incorporating non-Schmid effects into a discrete dislocation formulation was found to be critical for obtaining predictions consistent with experimental observations (Wang and Beyerlein, 2011). For rate independent continuum slip crystal plasticity Qin and Bassani (1992) developed a yield criterion incorporating non-Schmid stresses.

Here, we formulate a rate dependent continuum slip crystal plasticity constitutive relation that incorporates a non-Schmid shear stress term in a manner similar to Qin and Bassani (1992); Knezevic et al. (2014). The crystal plasticity formulation is the same as that of Peirce et al. (1983), which accounts for finite deformations, except for the non-Schmid stress components in the slip system flow rule. In the rate dependent formulation here, the non-Schmid stresses are taken to enter the driving force for slip and to act to reduce plastic deformation on the affected slip system or slip systems. One consequence of this can be a change in the slip mode. Another consequence is that with the inclusion of non-Schmid stresses in the plastic flow rule, a non-negative dissipation rate for all possible deformation histories is not guaranteed.

The requirement of a non-negative dissipation rate for all possible deformation histories, which is typically imposed on continuum plasticity formulations, is a constraint analogous to the postulate of Coleman and Noll (1964) that requires the Clausius-Duhem inequality to be satisfied for all possible deformation histories. However, within the context of statistical mechanics, satisfaction of the Clausius-Duhem inequality emerges in the limit of large systems and long times (Evans and Searles, 2002; Jarzynski, 2010). It can be violated for discrete events that take place for a short time period, see e.g. Evans and Searles (2002); Jarzynski (2010). Most reported violations of the Clausius-Duhem inequality concern atomic scale fluctuations, e.g. Wang et al. (2010), but Ostoja-Starzewski and Laudani (2020) observed violation of the Clausius-Duhem inequality even in a continuum scale discrete particle simulation.

For certain constitutive frameworks, satisfaction of the Clausius-Duhem inequality serves in some sense as a stability condition (Coleman and Mizel, 1967; Dafermos, 1979). However, for a viscoplastic solid, a simple one dimensional wave propagation calculation showed that a stable numerical calculation could be carried out with a negative dissipation rate occurring for a short period of time, but instability occurred with a sufficiently large negative dissipation rate, Needleman (2023). Because a non-Schmid slip system flow rule allows for the possibility of a negative dissipation rate, questions arise concerning the consequences of this, in particular: (i) what are the consequences, in a continuum slip crystal plasticity formulation, of the dissipation rate being negative (on a subset of the active slip systems or on all active slip systems)? (ii) what is the effect on stability if a negative dissipation rate does occur? and (iii), if so, are there conditions that can be imposed to ensure stability?

In addition to questions regarding the sign of the dissipation rate, the issues associated with a non-Schmid continuum slip formulation include: (i) what is the effect of non-Schmid stress governed plastic flow on the overall stress-strain response? and (ii) what effect does non-Schmid stress governed plastic flow have on the evolution of slip, particularly on the occurrence of localization of deformation?

Here, we investigate implications of non-Schmid governed plastic flow for continuum slip crystal plasticity in the context of quasi-static plane strain tension of a planar single crystal with two potentially active slip systems as analyzed by Peirce et al. (1983) for Schmid stress governed continuum slip plasticity. The crystal is oriented for symmetric double slip with the slip rate on one or both of the slip systems being affected by a non-Schmid stress which, for simplicity, is taken to be dependent on the Schmid resolved shear stress on the other slip system. Finite deformation, finite element analyses are carried out for planar tensile bars with an initial geometric imperfection to induce nonuniform deformations. The overall stress-strain response, including the onset of a rapid drop in overall stress due to the onset of localized deformation, and the evolution of the dissipation rate, both pointwise and integrated over the entire bar, are calculated for several characterizations of the non-Schmid stress term. The problem analyzed provides a simple context for investigating the consequences, if any, of a negative plastic dissipation rate.

2. Problem formulation

2.1. Crystal plasticity constitutive relation

The crystal plasticity constitutive relation used in the calculations follows Peirce et al. (1983) except for the slip system flow rule. For completeness, the basic equations are given here.

The deformation gradient $\mathbf{F}$ is written as

$$\mathbf{F} = \mathbf{F}^* \cdot \mathbf{F}^p \tag{1}$$

The plastic part of the deformation gradient, $\mathbf{F}^p$, results from slip occurring on crystallographic planes with normals $\mathbf{m}^{(\alpha)}$ and along directions $\mathbf{s}^{(\alpha)}$ on those plane, where α denotes the slip system. The elastic part of the deformation gradient, $\mathbf{F}^*$ is comprised of elastic deformation of the crystal lattice as well as any rigid body rotation.

Differentiating Eq. (1), with respect to time gives

$$\dot{\mathbf{F}} \cdot \mathbf{F}^{-1} = (\mathbf{D}^* + \boldsymbol{\Omega}^*) + (\mathbf{D}^p + \boldsymbol{\Omega}^p) \tag{2}$$

where $\dot{( )} = \partial( )/\partial t$, $(\mathbf{D}^* + \boldsymbol{\Omega}^*)$, is the elastic part of the rate of deformation tensor and the second term is the plastic part. The plastic stretching, $\mathbf{D}^p$, and spin tensors, $\boldsymbol{\Omega}^p$, are given by

$$\mathbf{D}^p = \sum_\alpha \dot{\gamma}^{(\alpha)} \mathbf{P}^{(\alpha)} \qquad \boldsymbol{\Omega}^p = \sum_\alpha \dot{\gamma}^{(\alpha)} \mathbf{W}^{(\alpha)} \tag{3}$$

with $\dot{\gamma}^{(\alpha)}$ the slip rate on slip system (α) (no implicit sum on repeated Greek indices) and

$$\mathbf{P}^{(\alpha)} = \frac{1}{2}(\mathbf{s}^{(\alpha)*}\mathbf{m}^{(\alpha)*} + \mathbf{m}^{(\alpha)*}\mathbf{s}^{(\alpha)*})$$

$$\mathbf{W}^{(\alpha)} = \frac{1}{2}(\mathbf{s}^{(\alpha)*}\mathbf{m}^{(\alpha)*} - \mathbf{m}^{(\alpha)*}\mathbf{s}^{(\alpha)*}) \tag{4}$$

where $\mathbf{s}^{(\alpha)*}$ and $\mathbf{m}^{(\alpha)*}$ are, respectively, the slip direction and slip plane normal in the current lattice configuration given by

$$\mathbf{s}^{(\alpha)*} = \mathbf{F}^* \cdot \mathbf{s}^{(\alpha)} \quad , \quad \mathbf{m}^{(\alpha)*} = \mathbf{m}^{(\alpha)} \cdot \mathbf{F}^{*-1} \tag{5}$$

The constitutive relation is written in terms of the Kirchhoff stress, $\boldsymbol{\tau} = \det(\mathbf{F})\boldsymbol{\sigma}$, with $\boldsymbol{\sigma}$ the Cauchy stress, and det( ) the determinant. Also, elasticity is assumed to be unaffected by slip and isotropic, and the elastic strains are assumed to remain small.

The lattice Jaumann rate of Kirchhoff stress, and the elastic rate of stretching are related by

$$\hat{\boldsymbol{\tau}}^* = \mathbf{L} : \mathbf{D}^* = \frac{E}{1+\nu}\left[\mathbf{D}^* + \frac{\nu}{1-2\nu}\mathrm{tr}(\mathbf{D}^*)\mathbf{I}\right] \tag{6}$$

where $\mathbf{L}$ is the tensor of elastic moduli, taken to be isotropic with E Young's modulus and ν Poisson's ratio. Also, tr( ) is the trace and $\mathbf{I}$ is the second order identity tensor.

The resulting expression for the material convected rate of Kirchhoff stress, $\dot{\boldsymbol{\tau}}^c$, is (Peirce et al., 1983)

$$\dot{\boldsymbol{\tau}}^c = \mathbf{L} : \mathbf{D} - \sum_\alpha \dot{\gamma}^{(\alpha)}\mathbf{R}^{(\alpha)} - \mathbf{D}\cdot\boldsymbol{\tau} - \boldsymbol{\tau}\cdot\mathbf{D} \tag{7}$$

with

$$\mathbf{R}^{(\alpha)} = \mathbf{L} : \mathbf{P}^{(\alpha)} + \mathbf{W}^{(\alpha)}\cdot\boldsymbol{\tau} - \boldsymbol{\tau}\cdot\mathbf{W}^{(\alpha)} \tag{8}$$

The extension of the rate independent yield strength expression of Qin and Bassani (1992) to rate dependent material behavior is taken to have the general form

$$\dot{\gamma}^{(\alpha)} = \dot{a}^{(\alpha)}\left(\frac{\chi^{(\alpha)}}{g^{(\alpha)}}\right) G\left[\left|\frac{\chi^{(\alpha)}}{g^{(\alpha)}}\right|\right] \tag{9}$$

where $\dot{a}^{(\alpha)}$ is a material constant, $g^{(\alpha)}$ is the hardness of slip system (α). $G[\cdot]$ is a specified function and

$$\chi^{(\alpha)} = \tau^{(\alpha)} + \sum_\kappa \lambda_{\alpha\kappa}\tau_{ns}^{(\kappa)} \tag{10}$$

with $\tau^{(\alpha)} = \mathbf{s}^{(\alpha)*}\cdot\boldsymbol{\tau}\cdot\mathbf{m}^{(\alpha)*}$ being the Schmid resolved shear stress on slip system (α), $\tau_{ns}^{(\kappa)}$ are specified non-Schmid stresses, and $\lambda_{\alpha\kappa}$ are specified constants. A relation of the form of Eq. (10) can incorporate other types of non-Schmid stress terms. For example, it can include normal stresses in addition to shear stresses so that a tension-compression asymmetry can be incorporated into the flow rule or it can include a back stress (with an appropriate back stress evolution expression).

In the calculations here, the slip rate $\dot{\gamma}^{(\alpha)}$ in Eq. (9) is given by the power law relation

$$\dot{\gamma}^{(\alpha)} = \dot{a}^{(\alpha)}\left(\frac{\chi^{(\alpha)}}{g^{(\alpha)}}\right)\left[\left|\frac{\chi^{(\alpha)}}{g^{(\alpha)}}\right|\right]^{(1/m-1)} = \dot{a}^{(\alpha)}\mathrm{sign}(\chi^{(\alpha)})\left[\left|\frac{\chi^{(\alpha)}}{g^{(\alpha)}}\right|\right]^{(1/m)} \tag{11}$$

In the special case where the only non-Schmid stresses associated with slip system (α) are the Schmid resolved shear stresses on other slip systems, Eq. (10) is written as

$$\chi^{(\alpha)} = \sum_{\kappa} c_{\alpha\kappa} \tau^{(\kappa)} \tag{12}$$

where $c_{\alpha\kappa}$ are specified constants, with the diagonal terms $c_{\alpha\alpha} = 1$.

The initial value of $g^{(\alpha)}$ is $\tau_0^{(\alpha)}$ and $g^{(\alpha)}$ evolves as

$$\dot{g}^{(\alpha)} = \sum_{\kappa} h_{\alpha\kappa} |\dot{\gamma}^{(\kappa)}| \tag{13}$$

The dissipation rate, $\dot{\xi}$, is given by

$$\dot{\xi} = \boldsymbol{\tau} : \mathbf{D}^p = \sum_{\alpha} \tau^{(\alpha)} \dot{\gamma}^{(\alpha)} = \sum_{\alpha} \dot{a}^{(\alpha)} \tau^{(\alpha)} \mathrm{sign}(\chi^{(\alpha)}) \left[\left| \frac{\chi^{(\alpha)}}{g^{(\alpha)}} \right| \right]^{(1/m)} \tag{14}$$

If $c_{\alpha\kappa} \equiv 0$, then $\chi^{(\alpha)} = \tau^{(\alpha)}$ and not only is $\dot{\xi}$ guaranteed to be non-negative but $\tau^{(\alpha)}\dot{\gamma}^{(\alpha)} \geq 0$ for all (α). With $\chi^{(\alpha)} \neq \tau^{(\alpha)}$ a non-negative dissipation rate is not guaranteed. It is expected that at least in some circumstances a negative dissipation rate leads to instability so we presume that some restriction needs to be imposed on the dissipation rate. However, precisely what restriction should be imposed remains to be determined.

In Eq. (11), the non-Schmid terms are incorporated into the driving force for slip in a manner similar to the formulation of Knezevic et al. (2014). This contrasts with the formulations of Weinberger et al. (2012); Lim et al. (2013); Chen et al. (2014); Srivastava et al. (2015); Asim et al. (2022) where non-Schmid stresses are incorporated into the hardness. The fundamental basis for the formulation in Eq. (11) is twofold: (i) in discrete dislocation plasticity, non-Schmid stress terms enters through the expression for dislocation velocity, see for example Needleman (2023, 2024); and (ii) the hardness is regarded as a material characteristic that depends on the state of the slip systems and not directly on the imposed loading (the evolution of the hardness does of course depend on the imposed loading). In discrete dislocation plasticity, the dissipation rate associated with dislocation K can be written as, see e.g. Needleman (2023),

$$\dot{\mathcal{D}}^K = \int_{L^K} P^K v^K dl \tag{15}$$

where the integration is over the dislocation line L^K, v^K is the dislocation velocity, and P^K is the Peach-Koehler (configurational) force given by

$$P^K = \bar{\tau}^K |\mathbf{b}^K| \tag{16}$$

with $\mathbf{b}^K$ the Burgers vector of dislocation K and $\bar{\tau}^K$ the total resolved shear stress minus the dislocation self-stress on the slip plane in the direction $\mathbf{b}^K$. The dislocation velocity can be specified by a relation of the form

$$v^K = \frac{1}{B^K} Q^K = \frac{1}{B^K} \left[P^K + \beta^K \tau_{ns}^K \right] \tag{17}$$

with B^K a specified constant. Then, Eq. (15) becomes

$$\dot{\mathcal{D}}^K = \int_{L^K} \left(\frac{1}{B^K} \right) P^K Q^K dl \tag{18}$$

If $\beta^K \neq 0$, $Q^K \neq P^K$ and a non-negative dissipation rate is not guaranteed. Thus, in discrete dislocation plasticity the Peach-Koehler force only involves the Schmid resolved shear stress and non-Schmid stresses enter the expression for the dissipation rate through their effect on the dislocation velocity. Eqs. (11) and (12) leading to Eq. (14) provide the continuum slip analog of this.

The inclusion of non-Schmid stresses of the form in Eq. (12) leads to a slight modification of the rate tangent expressions given by Peirce et al. (1983) for the constitutive integration. For completeness the modified expressions are given in the Appendix.

2.2. Boundary value problem formulation

The Lagrangian finite deformation finite element formulation is based on the quasi-static rate principle of virtual work that can be written as

$$\int_V \dot{\mathbf{s}} : \delta \mathbf{F} dV = \int_S \dot{\mathbf{T}} \cdot \delta \mathbf{u} dS + \left[\frac{1}{\Delta t} \left(\int_S \mathbf{T} \cdot \delta \mathbf{u} dS - \int_V \mathbf{s} : \delta \mathbf{F} dV \right) \right] \tag{19}$$

where $\mathbf{s}$ is the (unsymmetric) nominal stress tensor, $\mathbf{s} = \mathbf{F}^{-1} \cdot \boldsymbol{\tau}$, $\dot{\mathbf{T}} = \dot{\mathbf{s}} \cdot \mathbf{n}$, V is the volume of the body in the undeformed reference configuration, S is the corresponding surface with normal $\mathbf{n}$, and the deformation gradient $\mathbf{F}$ is related to the displacement vector $\mathbf{u}$ via

$$\mathbf{F} = \frac{\partial \mathbf{u}}{\partial \mathbf{X}} \quad , \quad \mathbf{u} = \mathbf{x} - \mathbf{X} \tag{20}$$

with $\mathbf{X}$ and $\mathbf{x}$ being the positions of a material point in the reference and current configurations, respectively. The term in brackets on the right hand side of Eq. (19) is an equilibrium correction term included in the calculations and Δt is the time increment.

Plane strain calculations of a planar single crystal subjected to tensile deformation (see Fig. 1a) are carried out using a convected coordinate formulation of the governing equations based on Eq. (19). Material particles are labeled by their position in the reference configuration, y^i, and these labels, together with time, serve as the set of independent variables. Time integration is carried out using a rate tangent method as in Peirce et al. (1983). For the sake of simplicity, the planar single crystal is assumed to have only two slip systems that are oriented symmetrically, as described in detail in the preceding Section 2.3.

Symmetry along both y^1 and y^2 axes is assumed, so that only one-fourth of the plane strain bar needs to be analyzed numerically, as shown in Fig. 1b. The bar analyzed is of length L_0 in the reference configuration and the width $w_0(y^2)$ in the reference configuration is given by

$$w_0(y^2) = \bar{w}_0 \left[1 - \rho \cos\left(\frac{\pi y^2}{L_0}\right)\right] \tag{21}$$

where y^i, $i = 1, 2$ are the coordinates of material points in the plane of deformation in the reference configuration, $\bar{w}_0$ is the nominal width and ρ is the imperfection amplitude.

A normal displacement is applied on $y^2 = L_0$ to give nominally constant strain rate loading

$$\dot{u}_2 = \dot{\varepsilon}_0 (U + L_0) \quad , \quad \dot{T}^1 = 0 \quad \text{on } y^2 = L_0 \tag{22}$$

Here, $\dot{u}_j$ $(j = 1, 2)$ are the in-plane displacement rates, $\dot{\varepsilon}_0$ is a specified applied strain rate, and U is the applied end displacement.

The side $y^1 = w_0(y^2)$ is taken to be traction free so that

$$\dot{T}^1 = 0 \quad \dot{T}^2 = 0 \quad \text{on } y^1 = w_0(y^2) \tag{23}$$

Symmetry conditions are imposed on $y^1 = 0$ and $y^2 = 0$ via

$$\dot{u}_1 = 0 \quad \dot{T}^2 = 0 \quad \text{on } y^1 = 0 \tag{24a}$$

$$\dot{u}_2 = 0 \quad \dot{T}^1 = 0 \quad \text{on } y^2 = 0 \tag{24b}$$

2.3. Planar crystal model

As in Peirce et al. (1983), the calculations are carried out for a planar model crystal with two slip systems (so that Greek indices range from 1 to 2) oriented symmetrically about the tensile axis with angles $\phi^{(1)} = \phi$ and $\phi^{(2)} = -\phi$. The initial slip directions are given by

$$\mathbf{s}^{(1)} = \cos\phi \mathbf{k}_1 + \sin\phi \mathbf{k}_2 \quad , \quad \mathbf{s}^{(2)} = \cos\phi \mathbf{k}_1 - \sin\phi \mathbf{k}_2 \tag{25}$$

where $\mathbf{k}_i$ are Cartesian base vectors in the initial configuration with $\mathbf{k}_2$ the tensile axis, see Fig. 1a. Note that with the traction in the $\mathbf{k}_2$ direction given by T^2, for uniform deformation the Schmid resolved shear stress on system (2) is given by $\tau^{(2)} = -T^2 \cos\phi \sin\phi$ so that with $\phi < \pi/2$, $\tau^{(2)}$ is negative for the symmetric double slip deformation mode.

The initial value of g is taken to be identical for both systems so that $g_0^{(1)} = g_0^{(2)} = \tau_0$ and in the calculations here χ^α is given by Eq. (12) with $c_{12} = c^{(1)} \text{sign}(\tau^{(1)}) \text{sign}(\tau^{(2)})$ and $c_{21} = c^{(2)} \text{sign}(\tau^{(2)}) \text{sign}(\tau^{(1)})$. Values $c^{(\alpha)} < 0$ result in a reduced driving force for slip regardless of the sign of $\tau^{(\alpha)}$.

The values of $c^{(\alpha)}$ are taken to depend on $\gamma^{(\beta)}$ so that

$$c^{(\alpha)} = c_{\text{amp}}^{(\alpha)} Z^{(\alpha)}(\gamma^{(\beta)}) \qquad \beta \neq \alpha \tag{26}$$

where $c_{\text{amp}}^{(\alpha)}$ is a specified constant, $(\alpha) \neq (\beta)$, and

$$Z^{(\alpha)}(\gamma^{(\beta)}) = \begin{cases} 0 & \text{for } |\gamma^{(\beta)}| \leq \gamma_b^{(\beta)} \\ \left| \sin\pi \left(\frac{|\gamma^{(\beta)}| - \gamma_b^{(\beta)}}{\gamma_e^{(\beta)}} \right) \right| & \text{for } \gamma_b^{(\beta)} \leq |\gamma^{(\beta)}| \leq \gamma_b^{(\beta)} + p^{(\beta)} \gamma_e^{(\beta)} \\ 0 & \text{for } \gamma_b^{(\beta)} + p^{(\beta)} \gamma_e^{(\beta)} \leq |\gamma^{(\beta)}| \end{cases} \tag{27}$$

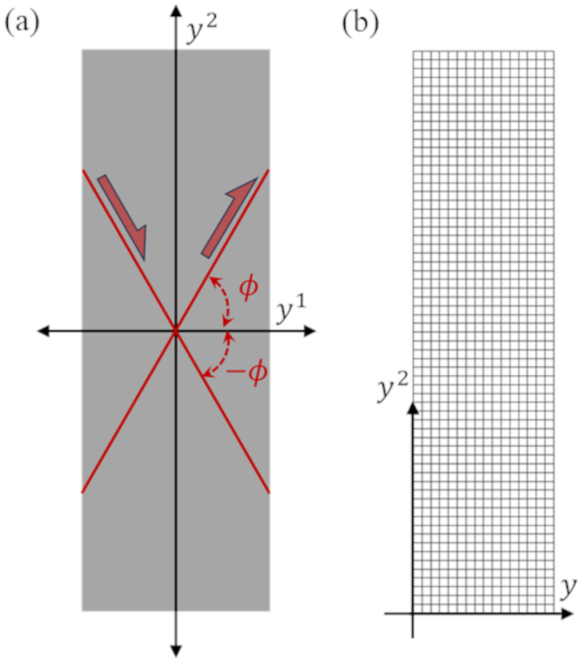

Figure 1: (a) Schematic representation of the crystal oriented for symmetric double slip. (b) The 16 × 64 quadrilateral element finite element mesh used in the calculations.

The variation of the non-Schmid effect during the loading history is expected to depend on the physical mechanism that give rise to the involvement of the non-Schmid stress component on plastic slip. For example, cross-slip would be expected to come into play for a relatively short time interval whereas any effect arising from the dislocation core structure would have an effect for a longer interval of the loading history. By varying $\gamma_b^{(\beta)}$, $\gamma_e^{(\beta)}$, and $p^{(\beta)}$, the onset and duration of either a single or repeated non-Schmid events can be represented in the simple double slip context. An example of the variation of $Z^{(\alpha)}$ with $\gamma^{(\beta)}$ as given by Eq. (27) and for $\gamma_b^{(\beta)} = 0.025$, $\gamma_e^{(\beta)} = 0.05$, and $p^{(\beta)} = 10$ is shown in Fig. 2a.

In order to limit the number of parameters considered, attention is restricted to self hardening that is the same for each slip system so that $h_{11} = h_{22} = h$ and $h_{12} = h_{21} = 0$. In the calculations here

$$h = h_0 \left(\frac{|\gamma^{(1)}| + |\gamma^{(2)}|}{\gamma_0 + 1} \right)^{N-1} \tag{28}$$

where γ_0 and N are specified constants. Calculations are carried out for various values of $c_{\mathrm{amp}}^{(\alpha)}$ in Eq. (26), and for various values of $\gamma_b^{(\beta)}$, $p^{(\beta)}$, and $\gamma_e^{(\beta)}$ in Eq. (27).

3. Results and discussion

All calculations are carried out for fixed values of $E/\tau_0 = 533.3$, $\nu = 0.3333$, $h_0/\tau_0 = 10$, $\gamma_0 = 0.01$, $N = 0.10$, $\dot{a}^{(1)} = \dot{a}^{(2)} = \dot{a} = 0.002/s$, and $m = 0.01$. The initial slip system

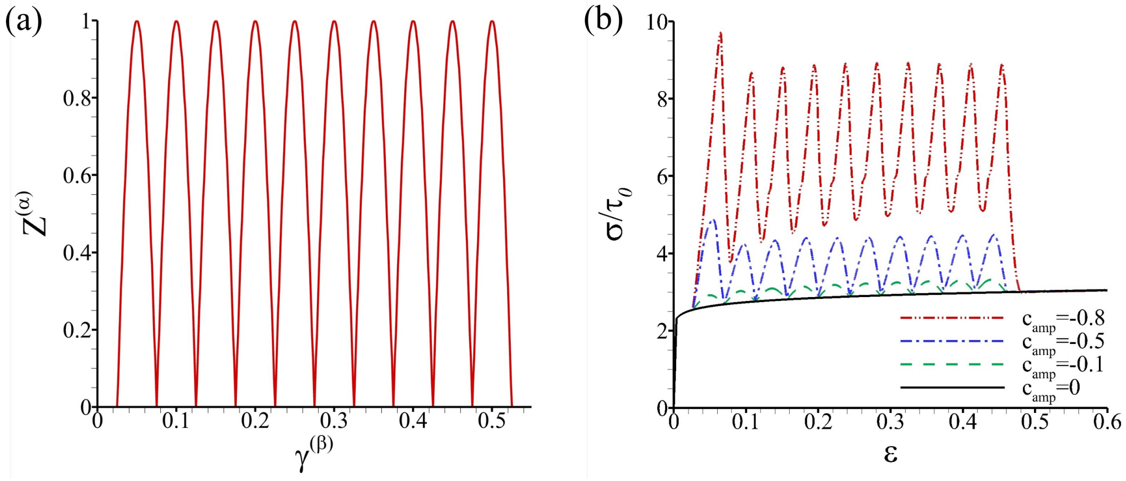

Figure 2: (a) An example of the variation of $Z^{(\alpha)}$ with $\gamma^{(\beta)}$ as given by Eq. (27) and for $\gamma_b^{(\beta)} = 0.025$, $\gamma_e^{(\beta)} = 0.05$, and $p^{(\beta)} = 10$ in Eq. (27). (b) Overall stress-strain response for uniform symmetric double slip with $\gamma_b^{(1)} = \gamma_b^{(2)} = 0.025$, $\gamma_e^{(1)} = \gamma_e^{(2)} = 0.05$, and $p^{(1)} = p^{(2)} = 10$ in Eq. (27) and with various values of $c_{\rm amp}^{(1)} = c_{\rm amp}^{(2)} = c_{\rm amp}$. The definition of σ and ε are given in Section. 3.1.

orientations are specified to be $\phi = \pi/3$ and the bar aspect ratio is $\bar{w}_0/L_0 = 0.25$. In all calculations, the imposed loading rate in Eq. (22) is given by $\dot{\varepsilon}_0/\dot{a} = 1$. For comparison purposes some calculations are carried out for a uniform bar, $\rho = 0$ in Eq. (21), but in most calculations the imperfection amplitude, ρ, is taken to be $\rho = 0.01$. Unless specifically stated otherwise, calculations are carried out using a 16×64 quadrilateral element mesh, as shown in Fig. 1b, with each quadrilateral consisting of four crossed triangles. The finite element mesh is nearly uniform (when $\rho = 0$) with mesh spacing in the y^1-direction being $w_0(y^2)/16$ and in the y^2-direction being $L_0/64$.

3.1. Uniform non-Schmid governed slip

With $\rho = 0$ in Eq. (21) and $c_{\rm amp}^{(1)} = c_{\rm amp}^{(2)} = c_{\rm amp}$, the deformation mode is one of uniform symmetric double slip. Fig. 2b shows the computed overall stress-strain curves for various values of $c_{\rm amp}$ with the parameters in Eq. (27) taken as stated in the caption of Fig. 2b. The overall strain is defined as $\varepsilon = \ln(1 + U/L_0)$, where U is the applied end displacement in Eq. (22) and σ is given by

$$\sigma = \left(\frac{1}{[w(L_0) + u_1(w(L_0), L_0)]} \right) \int_0^{w(L_0)} T^2 dy^1 \tag{29}$$

where $[w(L_0) + u_1(w(L_0), L_0)]$ is the width of the bar at $y^2 = L_0$ and the integral gives the total force in the y^2-direction.

With the boundary conditions imposed, there is no uniform or homogeneous deformation solution with $c^{(1)} \neq c^{(2)}$. From Eqs. (11) and (12), the effect of activating the non-Schmid dependence is to reduce the driving force for plastic slip, so that the slip rate decreases and the hardening rate increases. For symmetric double slip, the overall stress-strain response reflects the periodicity of $Z^{(\alpha)}$ in Eq. (27). As the amplitude of negative c_{amp} increases the stress magnitude increases, for example with $c_{\text{amp}} = -0.8$, the stress magnitude is more than three times the stress magnitude attained with $c_{\text{amp}} = 0$.

The formulation here is rate dependent, so that a loss of ellipticity does not occur. However, for $m \rightarrow 0$ with a fixed non-zero Δt, the acoustic tensor based on the rate tangent modulus, $\mathbf{L}^{\tan}$, in Eq. (A-14) can give rise to imaginary wave speeds. This does occur for the calculation in Fig. 2b with $c_{\text{amp}} = -0.8$, while for $c_{\text{amp}} \geq -0.5$ these calculated (numerical) wave speeds remain real. Although loss of ellipticity does not occur, the governing equations can become ill-conditioned in such a case and, for a given Δt, lead to numerical stability and accuracy issues as discussed by Needleman (1988). Increasing strain rate hardening and decreasing numerical time step sizes all promote numerical stability in this sense. In addition to loss of ellipticity, a flutter instability is possible with a nonassociative flow rule, due to the stiffness matrix relating the nominal stress and the deformation gradient (or rates thereof) being non-symmetric, Piccolroaz et al. (2006). In addition, deformation of a rate dependent plastic solid for which the flow rule for the limiting rate independent solid is nonassociative can exhibit intermittent strain bursts, Racherla and Bassani (2007); Bassani and Racherla (2011).

3.2. Uniform and nonuniform Schmid governed slip

Fig. 3a shows the stress-strain responses for Schmid governed slip, $c^{(1)} = c^{(2)} = 0$ in Eq. (26). With $\rho = 0$, the response is spatially uniform symmetric double slip. In the early stages of deformation, there is little difference between the overall stress-strain responses with $\rho = 0$ and $\rho = 0.01$ in Eq. (21). Once necking begins, Fig. 3b, the deformation field with $\rho = 0.01$ is highly nonuniform and the overall stress, σ, decreases with increasing imposed displacement. The deformation eventually localizes leading to a rapid drop in overall stress. We term the strain at which such a rapid drop in overall stress occurs the failure strain and denote it by ε_f.

The variation of the overall normalized dissipation rate with strain is shown in Figs. 3c and 3d, where the overall normalized dissipation rate for slip system (α) is defined by

$$\dot{D}^{(\alpha)} = \left(\frac{1}{\tau_0 \dot{a}}\right) \int_{A_0} \tau^{(\alpha)} \dot{\gamma}^{(\alpha)} dA = \left(\frac{1}{\tau_0 \dot{a}}\right) \int_{A_0} \dot{\xi}^{(\alpha)} dA \tag{30}$$

where A_0 is the initial area of the bar and $\dot{\xi}^{(\alpha)}$ is the pointwise dissipation rate of slip system (α).

The values of $\dot{D}^{(1)}$ for uniform symmetric double slip, $\rho = 0$, and for $\rho = 0.01$ in Fig. 3c nearly coincide until the onset of localization, at which strain, the dissipation rate for the calculation with $\rho = 0.01$ increases rapidly. On the other hand in Fig. 3d for $\dot{D}^{(1)} + \dot{D}^{(2)}$, the difference between uniform symmetric double slip and the nonuniform deformation field that emerges with $\rho = 0.01$ occurs for much smaller values of overall strain, indicating that the nonuniform deformation field gives rise to more slip on slip system (1) than on slip system (2) until the onset of localization when the dissipation rate for both systems

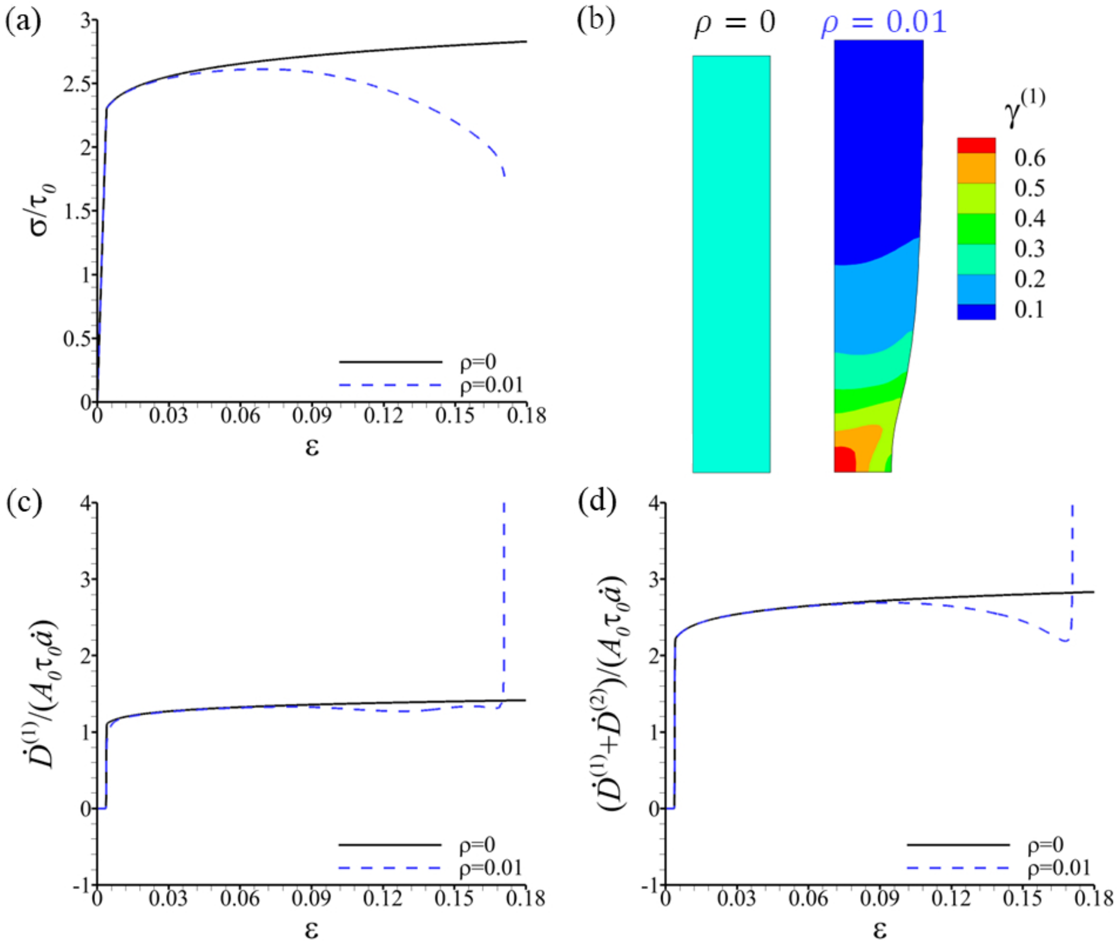

Figure 3: (a) Overall stress-strain response for Schmid stress governed slip in the plane strain bars with imperfection amplitude of $\rho = 0$ or $\rho = 0.01$. (b) The deformed shape of 1/4 of the plane strain bars at an imposed overall strain of $\varepsilon = 0.15$. The contour plot in (b) shows the variation of slip (γ) on slip system (1). The variation of slip on slip system (2) for the cases shown in (b) is the same but with a minus sign. (c)-(d) Normalized dissipation rate $\dot{D}^{(\alpha)}$ given by Eq. (30) for Schmid stress governed slip: (c) For slip system (1), and (d) for slip systems (1)+(2).

increases rapidly. Due to the rapidly localizing deformation, the time step for numerical stability becomes extremely small and the calculation is terminated.

3.3. Nonuniform non-Schmid governed slip

We first consider cases where there is a single interval of slip over which non-Schmid governed slip occurs, i.e., $p^{(1)} = p^{(2)} = 1$ in Eq. (27). Figs. 4a and 4b show overall stress-strain responses for various values of $c^{(1)}_{\rm amp}$ when $c^{(2)}_{\rm amp} = 0$ and when $c^{(1)}_{\rm amp} = c^{(2)}_{\rm amp} = c_{\rm amp}$, respectively, with $\gamma_e^{(1)} = \gamma_e^{(2)} = 0.02$. With $c^{(2)}_{\rm amp} = 0$, Fig. 4a, there is a relatively small effect of the non-Schmid term on the overall stress-strain response even with $c^{(1)}_{\rm amp} = -2$ although

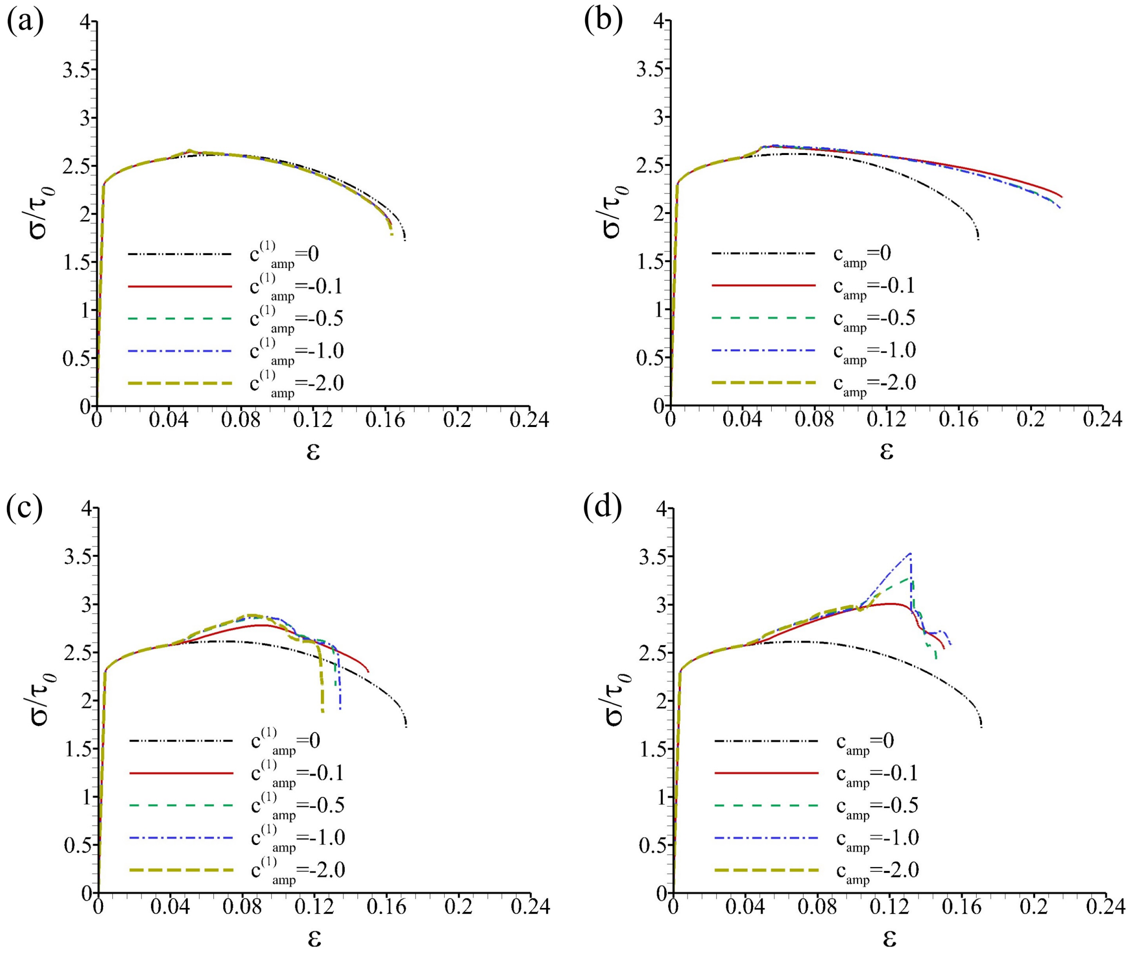

Figure 4: Overall stress-strain response for cases with (a) $\gamma_e^{(1)} = \gamma_e^{(2)} = 0.02$, $c_{\text{amp}}^{(2)} = 0$, and various values of $c_{\text{amp}}^{(1)}$; (b) $\gamma_e^{(1)} = \gamma_e^{(2)} = 0.02$, and various values of $c_{\text{amp}}^{(1)} = c_{\text{amp}}^{(2)} = c_{\text{amp}}$; (c) $\gamma_e^{(1)} = \gamma_e^{(2)} = 0.2$, $c_{\text{amp}}^{(2)} = 0$, and various values of $c_{\text{amp}}^{(1)}$; and (d) $\gamma_e^{(1)} = \gamma_e^{(2)} = 0.2$, and various values of $c_{\text{amp}}^{(1)} = c_{\text{amp}}^{(2)} = c_{\text{amp}}$. For all cases in (a)-(d), $\gamma_b^{(1)} = \gamma_b^{(2)} = 0.05$ and $p^{(1)} = p^{(2)} = 1$ in Eq. (27).

there is a small decrease in the value of the failure strain, ε_f, relative to that when plastic flow is governed only by the Schmid stress. On the other hand, when $c_{\text{amp}}^{(1)} = c_{\text{amp}}^{(2)}$, Fig. 4b, the effect of the non-Schmid term is to increase the stress magnitude and delay the onset of failure, with nearly no dependence on the value of c_{amp} for $-1 \leq c_{\text{amp}} < 0$. However, when the value of c_{amp} is very large, e.g., $c_{\text{amp}} = -2$, although the overall stress-strain curve initially follows the other curves for non-Schmid governed slip, the calculation terminates at $\varepsilon \approx 0.05$ because the time step required for numerical stability becomes extremely small. All other cases shown in Figs. 4a and 4b terminate after the localization of deformation, leading to a drop in overall stress.

With $\gamma_e^{(1)} = \gamma_e^{(2)} = 0.2$ in Figs. 4c and 4d, there is a very strong effect of the non-Schmid term on the overall stress-strain response both for $c_{\text{amp}}^{(1)} \neq 0$ and $c_{\text{amp}}^{(2)} = 0$ (Fig. 4c), and

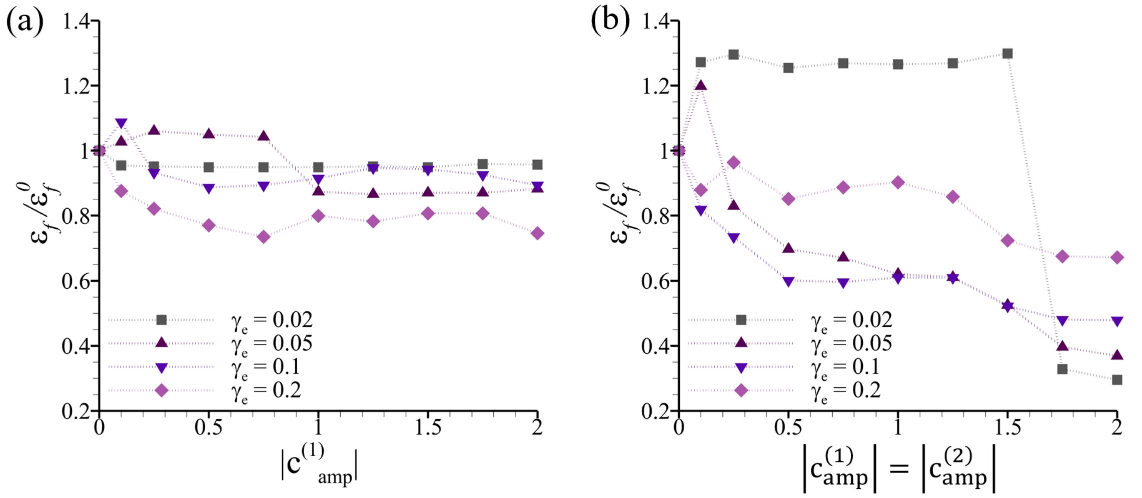

Figure 5: The variation of strain to failure, ε_f, with the magnitude of the non-Schmid parameter, (a) $c^{(1)}_{\text{amp}}$ when $c^{(2)}_{\text{amp}} = 0$, and (b) $c^{(1)}_{\text{amp}} = c^{(2)}_{\text{amp}} = c_{\text{amp}}$, for various values of $\gamma^{(1)}_e = \gamma^{(2)}_e = \gamma_e$. For all cases in (a)-(b), $\gamma^{(1)}_b = \gamma^{(2)}_b = 0.05$ and $p^{(1)} = p^{(2)} = 1$ in Eq. (27). The normalization parameter ε^0_f is the strain to failure for Schmid stress-governed slip.

for $c^{(1)}_{\text{amp}} = c^{(2)}_{\text{amp}} = c_{\text{amp}}$ (Fig. 4d). For both cases, there is a significant increase in stress magnitude due to the activation of the non-Schmid term, along with a significant decrease in the value of the overall strain at which a rapid drop in stress magnitude occurs. In Fig. 4c, where $c^{(2)}_{\text{amp}} = 0$, the increase in the stress magnitude (beyond the Schmid governed case) with increasing magnitude of $c^{(1)}_{\text{amp}}$ is rather small for the range of values of $c^{(1)}_{\text{amp}}$ considered. However, with $c^{(1)}_{\text{amp}} = c^{(2)}_{\text{amp}} = c_{\text{amp}}$ in Fig. 4d, a secondary increase in the hardening rate occurs for $c_{\text{amp}} \leq -0.5$ at $\varepsilon > 0.1$, where the overall stress increases almost linearly with increasing overall strain. All the cases shown in Figs. 4c and 4d terminate after a drop in overall stress occurs, except for $c_{\text{amp}} = -2$ in Fig. 4d, where the time step required for numerical stability becomes extremely small even before the drop in overall stress.

Fig. 5 shows the effect of the magnitude of the non-Schmid term, $|c^{(1)}_{\text{amp}}|$ and $c^{(2)}_{\text{amp}} = 0$ (Fig. 5a) and with $|c^{(1)}_{\text{amp}}| = |c^{(2)}_{\text{amp}}|$ (Fig. 5b) on the strain to failure, ε_f. In all cases shown in Fig. 5, $\gamma^{(1)}_b = \gamma^{(2)}_b = 0.05$, $p^{(1)} = p^{(2)} = 1$, and $\gamma^{(1)}_e = \gamma^{(2)}_e = \gamma_e$ in Eq. (27). In most calculations, ε_f corresponds to the value of the overall strain at which the calculations terminate due to a rapid drop in overall stress. However, with $|c^{(1)}_{\text{amp}}| = |c^{(2)}_{\text{amp}}| \geq 1.5$, calculations can be terminated because the time step required for numerical stability becomes extremely small before the drop in overall stress. A comparison of Fig. 5a and Fig. 5b shows that the value of ε_f has a much stronger dependence on the magnitude of the non-Schmid term when it is active on both slip systems (Fig. 5b) compared to when it is active on only one slip system (Fig. 5a). For example, when the non-Schmid is active on only one slip system, the maximum increase in ε_f is only 8% (for $\gamma_e = 0.1$ and $|c^{(1)}_{\text{amp}}| = 0.1$), and the maximum decrease in ε_f is roughly 24% (for $\gamma_e = 0.2$ and $|c^{(1)}_{\text{amp}}| = 0.75$). However, when the non-Schmid term is active on both slip systems, the maximum increase in ε_f is about 25% (for $\gamma_e = 0.02$ and $|c_{\text{amp}}^{(1)}| = |c_{\text{amp}}^{(2)}| = 0.25$), and the maximum decrease in ε_f is about 70% (for $\gamma_e = 0.02$ and $|c_{\text{amp}}^{(1)}| = |c_{\text{amp}}^{(2)}| = 2$). Furthermore, both when the non-Schmid term is active on one or on both slip systems, the variation of ε_f with γ_e is not necessarily monotonic. For example, in Fig. 5a, ε_f for $\gamma_e = 0.05$ is greater than that for $\gamma_e = 0.02$ when $|c_{\text{amp}}^{(1)}| < 1$ and the reverse holds when $|c_{\text{amp}}^{(1)}| > 1$.

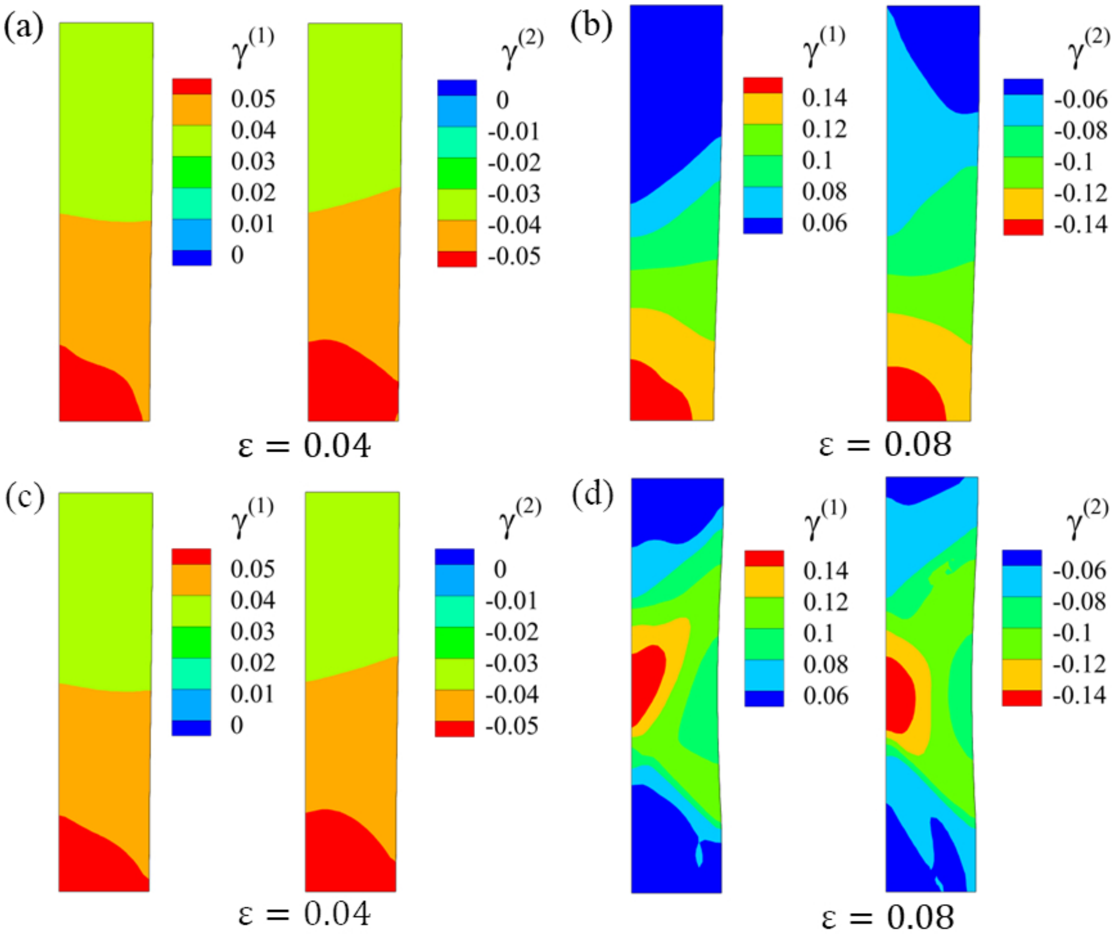

Figure 6: (a)-(b) Contour plots showing the distribution of slip (γ) on slip systems (1) and (2) for $c_{\text{amp}}^{(1)} = -0.1$ when $c_{\text{amp}}^{(2)} = 0$ at overall strain magnitudes of 0.04 and 0.08. (c)-(d) Contour plots showing the distribution of γ on slip systems (1) and (2) for $c_{\text{amp}}^{(1)} = c_{\text{amp}}^{(2)} = -0.1$ at overall strain magnitudes of 0.04 and 0.08. In both the cases, $\gamma_b^{(1)} = \gamma_b^{(2)} = 0.05$, $\gamma_e^{(1)} = \gamma_e^{(2)} = 0.02$, and $p^{(1)} = p^{(2)} = 1$ in Eq. (27).

The contour plots in Fig. 6 show the distribution of slip on the two slip systems (1) and (2) at two values of ε for two cases: one with $c_{\text{amp}}^{(1)} = -0.1$ (and $c_{\text{amp}}^{(2)} = 0$), and the other with $c_{\text{amp}}^{(1)} = c_{\text{amp}}^{(2)} = -0.1$. The values of the other parameters in Eq. (27) are given in the figure caption. Non-Schmid governed slip on a slip system (β) is only active when

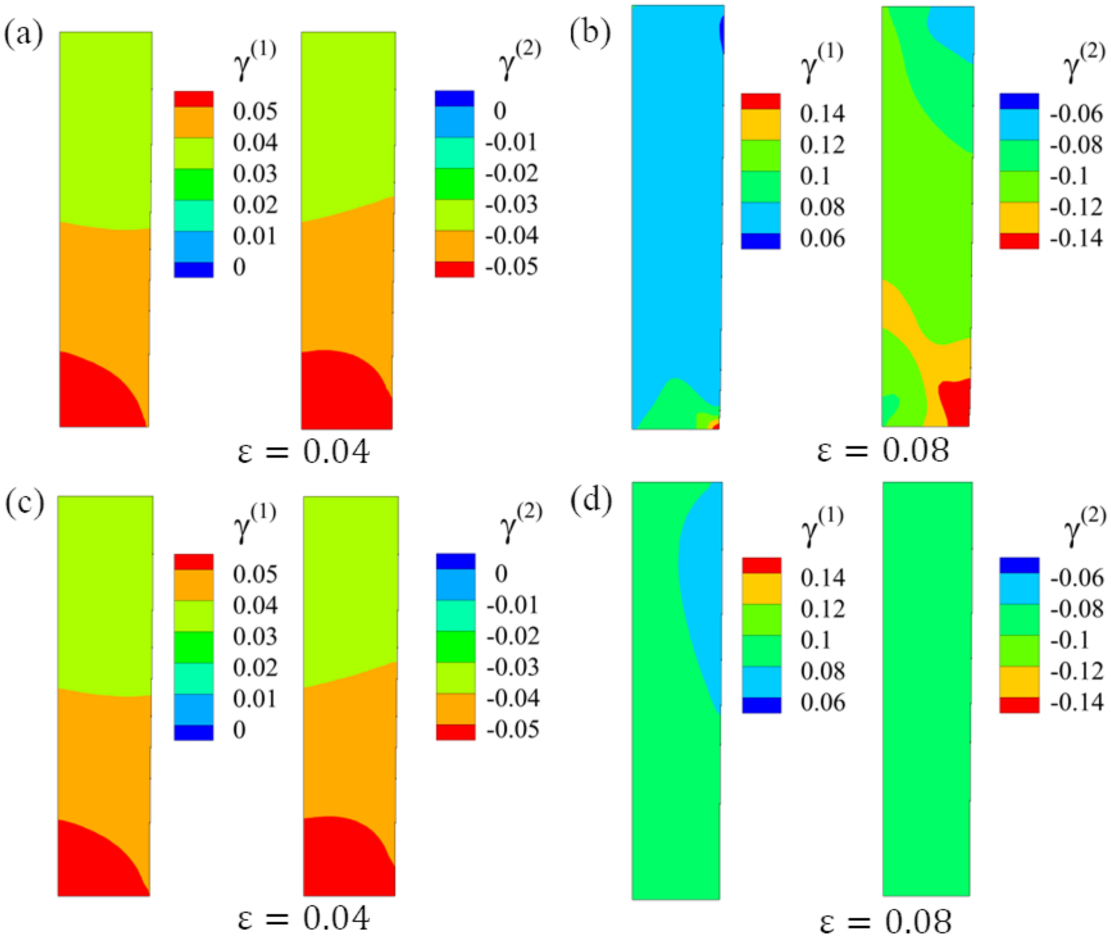

Figure 7: Similar contour plots to those in Fig. 6, but with $\gamma_e^{(1)} = \gamma_e^{(2)} = 0.2$ (increased from 0.02), while $\gamma_b^{(1)} = \gamma_b^{(2)} = 0.05$ and $p^{(1)} = p^{(2)} = 1$ remain unchanged. (a)-(b) Contour plots showing the distribution of γ on slip systems (1) and (2) for $c_{\rm amp}^{(1)} = -0.1$ when $c_{\rm amp}^{(2)} = 0$ at overall strain magnitudes of 0.04 and 0.08. (c)-(d) Contour plots showing the distribution of γ on slip systems (1) and (2) for $c_{\rm amp}^{(1)} = c_{\rm amp}^{(2)} = -0.1$ at overall strain magnitudes of 0.04 and 0.08.

$\gamma_b^{(\beta)} \leq |\gamma^{(\beta)}| \leq \gamma_b^{(\beta)} + p^{(\beta)}\gamma_e^{(\beta)}$. Therefore, for the values of γ_b and γ_e considered, at $\varepsilon = 0.04$, non-Schmid governed slip has not yet been activated, while at $\varepsilon = 0.08$, non-Schmid governed slip has been deactivated, at least in regions with sufficiently large values of $|\gamma^{(\beta)}|$. As a consequence, in all four sub-figures of Fig. 6, the deformation mode is nearly symmetric double slip.

The overall stress-strain response for the calculations in Fig. 6 are shown in Figs. 4a and 4b. The overall stress-strain response in Fig. 4a with $c_{\rm amp}^{(1)} = -0.1, c_{\rm amp}^{(2)} = 0$ differs little from the overall stress-strain response with $c_{\rm amp}^{(1)} = c_{\rm amp}^{(2)} = 0$. On the other hand, Fig. 4b shows that with $c_{\rm amp}^{(1)} = c_{\rm amp}^{(2)} = c_{\rm amp} = -0.1$ the stress magnitudes are greater for $\varepsilon > 0.05$ than the corresponding stress magnitudes with $c_{\rm amp}^{(1)} = c_{\rm amp}^{(2)} = c_{\rm amp} = 0$. Also, the values of ε_f with

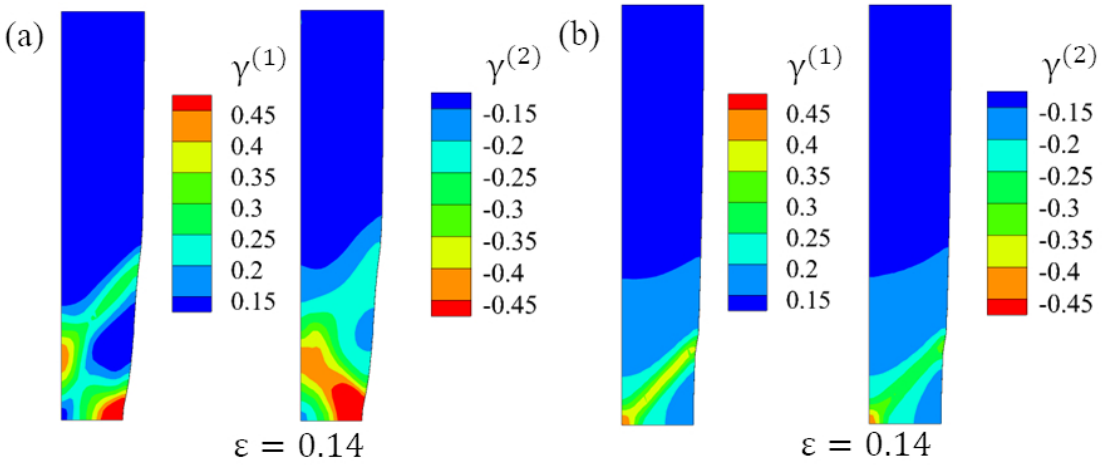

Figure 8: Contour plots showing the distribution of γ on slip systems (1) and (2) for the same cases shown in Fig. 7 but at a larger overall strain magnitude of 0.14. (a) For $c^{(1)}_{\rm amp} = -0.1$ when $c^{(2)}_{\rm amp} = 0$, and (b) for $c^{(1)}_{\rm amp} = c^{(2)}_{\rm amp} = -0.1$.

$c^{(1)}_{\rm amp} = c^{(2)}_{\rm amp} = c_{\rm amp} = -0.1$ are significantly greater than those with Schmid stress governed slip. The slip distributions in Fig. 6 show that this is due to the difference in the mode of deformation when non-Schmid governed slip is active on one slip system as compared with when non-Schmid stress governed slip is active on both slip systems. When non-Schmid stress governed slip is active on one slip system, the deformation pattern in the bar, shown in Fig. 6b, is similar to the case with Schmid stress governed slip, where necking occurs at the location of the minimum cross-section (see Fig. 3b). However, with non-Schmid governed slip active on both slip systems, necking does not occur at the minimum cross-section but occurs in the middle of the analyzed region of the bar, as shown in Fig. 6d. Because the region shown in Fig. 6 represents only one-fourth of the entire plane strain tensile bar, this suggests that even under quasi-static loading conditions, more than one neck can form in the bar due to non-Schmid stress governed slip.

Plots of the slip distribution with $\gamma^{(1)}_e = \gamma^{(2)}_e = 0.2$ are shown in Fig. 7. Here, as in Fig. 6 (where $\gamma^{(1)}_e = \gamma^{(2)}_e = 0.02$), plots are shown for $c^{(1)}_{\rm amp} = -0.1$, $c^{(2)}_{\rm amp} = 0$ and for $c^{(1)}_{\rm amp} = c^{(2)}_{\rm amp} = -0.1$. Also, the plots in Fig. 7 are at the same two values of ε as are the plots in Fig. 6. The values of the other parameters of Eq. (27) are given in the figure caption. With the specified values of γ_b and γ_e, the non-Schmid term has not yet been activated at $\varepsilon = 0.04$. As a result, at this magnitude of overall strain, the deformation is nearly symmetric double slip, as seen in Figs. 7a and 7c. At $\varepsilon = 0.08$, however, the non-Schmid term is active, leading to a change in deformation pattern: with $c^{(1)}_{\rm amp} = -0.1$ and $c^{(2)}_{\rm amp} = 0$ the deformation on slip system (1) is nearly suppressed. On the other hand, with $c^{(1)}_{\rm amp} = c^{(2)}_{\rm amp} = -0.1$, the deformation remains nearly symmetric double slip, but slip activity on both slip systems is suppressed. This results in increased stress magnitudes both with $c^{(2)}_{\rm amp} = 0$ and with $c^{(2)}_{\rm amp} = -0.1$ as compared to the corresponding stress magnitudes for Schmid governed slip

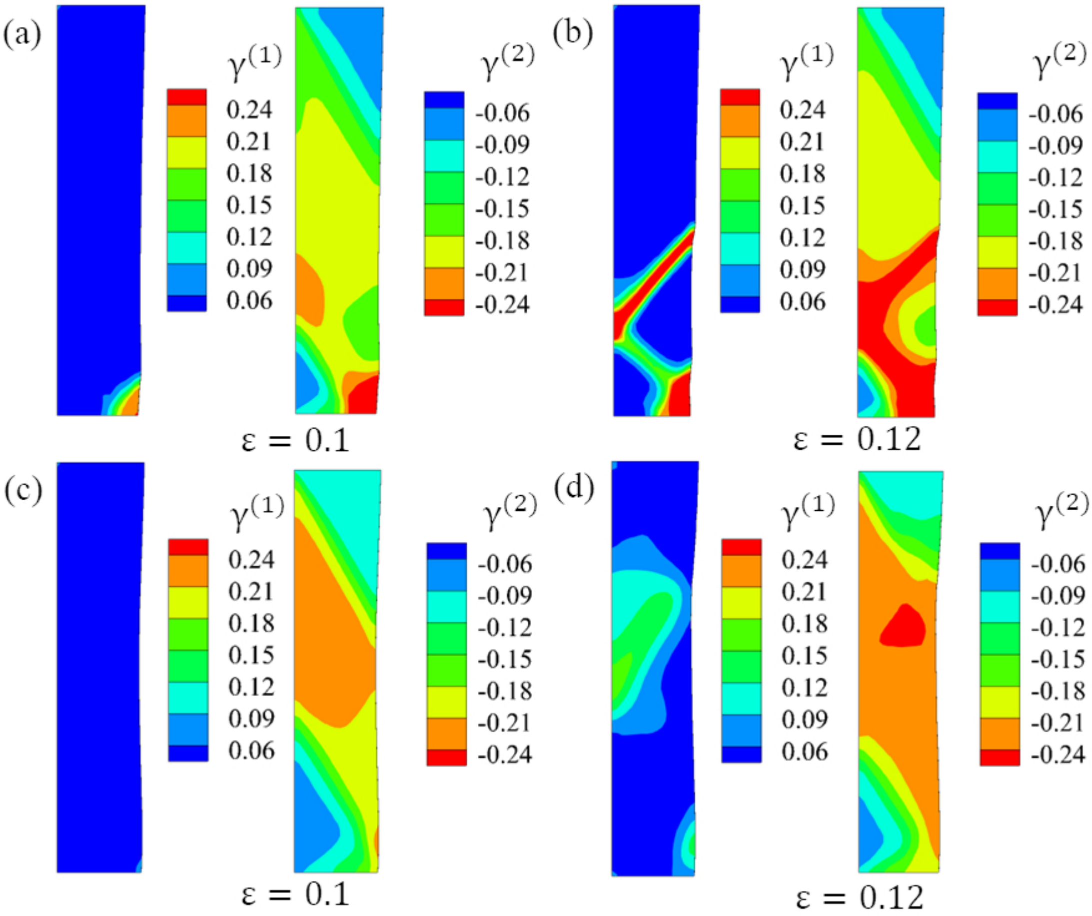

Figure 9: Contour plots showing the distribution of γ on slip systems (1) and (2) for (a)-(b) $c_{\text{amp}}^{(1)} = -1$ when $c_{\text{amp}}^{(2)} = 0$, and (c)-(d) for $c_{\text{amp}}^{(1)} = c_{\text{amp}}^{(2)} = -1$ at overall strain magnitudes of 0.1 and 0.12. In both cases, $\gamma_b^{(1)} = \gamma_b^{(2)} = 0.05$, $\gamma_e^{(1)} = \gamma_e^{(2)} = 0.2$, and $p^{(1)} = p^{(2)} = 1$ in Eq. (27).

when $\varepsilon > 0.05$, Figs. 4c and 4d. The stress magnitudes are greater when the non-Schmid term is activated on both slip systems as compared with when it is activated on only one slip system. Additionally, as seen in Figs. 4c and 4d, the values of ε_f for both cases with non-Schmid stress governed slip is significantly lower than for the case with Schmid stress governed slip. This is because with non-Schmid stress governed slip, as the imposed overall strain increases, deformation localizes in slip bands, as seen in Fig. 8. However, the pattern of slip localization differs between the cases with $c_{\text{amp}}^{(1)} = -0.1$ ($c_{\text{amp}}^{(2)} = 0$) in Fig. 8a, and with $c_{\text{amp}}^{(1)} = c_{\text{amp}}^{(2)} = -0.1$ in Fig. 8b.

Fig. 9 shows slip distributions for two cases with $c_{\text{amp}}^{(1)} = -1$. In one case $c_{\text{amp}}^{(2)} = 0$ and in the other case $c_{\text{amp}}^{(2)} = -1$. For both cases, all parameters in Eq. (27) are the same as in Figs. 7 and 8. In Fig. 9, at $\varepsilon = 0.1$, the deformation on slip system (1) is nearly suppressed, and the minimum cross-section in the current configuration is not at the location of the minimum cross-section in the initial configuration. For both cases, this results in increased stress magnitudes compared with the Schmid governed slip response in Figs. 4c and 4d. The stress magnitudes are greater when $c^{(1)}_{\rm amp} = c^{(2)}_{\rm amp} = -1$ than with only $c^{(1)}_{\rm amp} = -1$ (see Figs. 4c and 4d). This is because slip activity is much more suppressed when $c^{(2)}_{\rm amp} = -1$ than when $c^{(2)}_{\rm amp} = 0$. Furthermore, for $\varepsilon > 0.1$ with $c^{(1)}_{\rm amp} = c^{(2)}_{\rm amp} = -1$ the overall stress increases almost linearly with increasing strain until a rapid drop in overall stress occurs, as seen in Fig. 4d. This is because, even with increasing overall strain, slip activity remains rather suppressed and no slip bands form when $c^{(1)}_{\rm amp} = c^{(2)}_{\rm amp} = -1$, Fig. 9d. In contrast, when $c^{(2)}_{\rm amp} = 0$, deformation localizes into slip bands, as seen in Fig. 9b. In Fig. 9c and 9d even with $c^{(1)}_{\rm amp} = c^{(2)}_{\rm amp} = -1$, slip activity is not the same on the two slip systems. This is because the difference between non-Schmid governed plastic flow on only one slip system versus on both slip systems depends on the complex changes in the deformation mode of the bar.

The variation of various measures of dissipation rate with overall strain, ε, is shown in Fig. 10 for cases with $\gamma^{(1)}_b = \gamma^{(2)}_b = 0.05$, $\gamma^{(1)}_e = \gamma^{(2)}_e = 0.02$, $p^{(1)} = p^{(2)} = 1$, $c^{(2)}_{\rm amp} = 0$, and various values of $c^{(1)}_{\rm amp}$. The overall stress-strain responses for these cases are shown in Fig. 4a. The variation of the normalized dissipation rate $\dot{D}^{(1)}/(A_0\tau_0\dot{a})$ with ε is shown in Fig. 10a and the variation of the sum $(\dot{D}^{(1)} + \dot{D}^{((2)})/(A_0\tau_0\dot{a})$ is shown in Fig. 10b. When the non-Schmid term comes into play, the dissipation rate for system (1) decreases because of the decreased driving force for slip on that system. After the non-Schmid event has ended, the resistance to slip decreases and the dissipation rate on system (1) increases. As ε increases, the dissipation rate on system (1) becomes nearly independent of ε until the overall stress drops rapidly as deformation localizes. This leads to a sharp increase in the dissipation rate on system (1). By way of contrast, the value of the total dissipation rate $\dot{D} = \dot{D}^{(1)} + \dot{D}^{(2)}$ is nearly independent of the value of $c^{(1)}_{\rm amp}$ until $\varepsilon = \varepsilon_f$. This is because the value of $\dot{D}^{(2)}$ changes to balance out the change in $\dot{D}^{(1)}$. Also, the value of $\dot{D}^{(\alpha)}$ is non-negative throughout the deformation history up to and including $\varepsilon = \varepsilon_f$.

Figs. 10c and 10d show the minimum values of normalized pointwise dissipation rate $\dot{\xi}^{(1)}$ and $\dot{\xi}^{(1)} + \dot{\xi}^{(2)}$. The minimum values of both dissipation rate measures can become negative. Note that the values shown are the minimum value of the dissipation rate in the bar and so the point at which this minimum occurs can vary from time step to time step. Hence, the associated curve can have strong oscillations. Also, for ε greater than about 0.12, the minimum values are zero because elastic unloading has occurred and at all points where slip is occurring the dissipation rates are non-negative. These results show that strongly negative values of pointwise dissipation rate, $\dot{\xi}^{(\alpha)}$, can occur with the overall response remaining stable.

Fig. 11 shows the evolution of normalized dissipation rate for calculations with all parameters as in the cases in Fig. 10 except that here $c^{(1)}_{\rm amp} = c^{(2)}_{\rm amp} = c_{\rm amp}$. The overall stress-strain responses for these cases are shown in Fig. 4b. The qualitative behavior is similar with non-negative values of $\dot{D}^{(\alpha)}$ and with values of the pointwise dissipation rate $\dot{\xi}^{(\alpha)}$ attaining locally negative values.

The evolution of normalized dissipation rate is quite different for the cases in Fig. 12

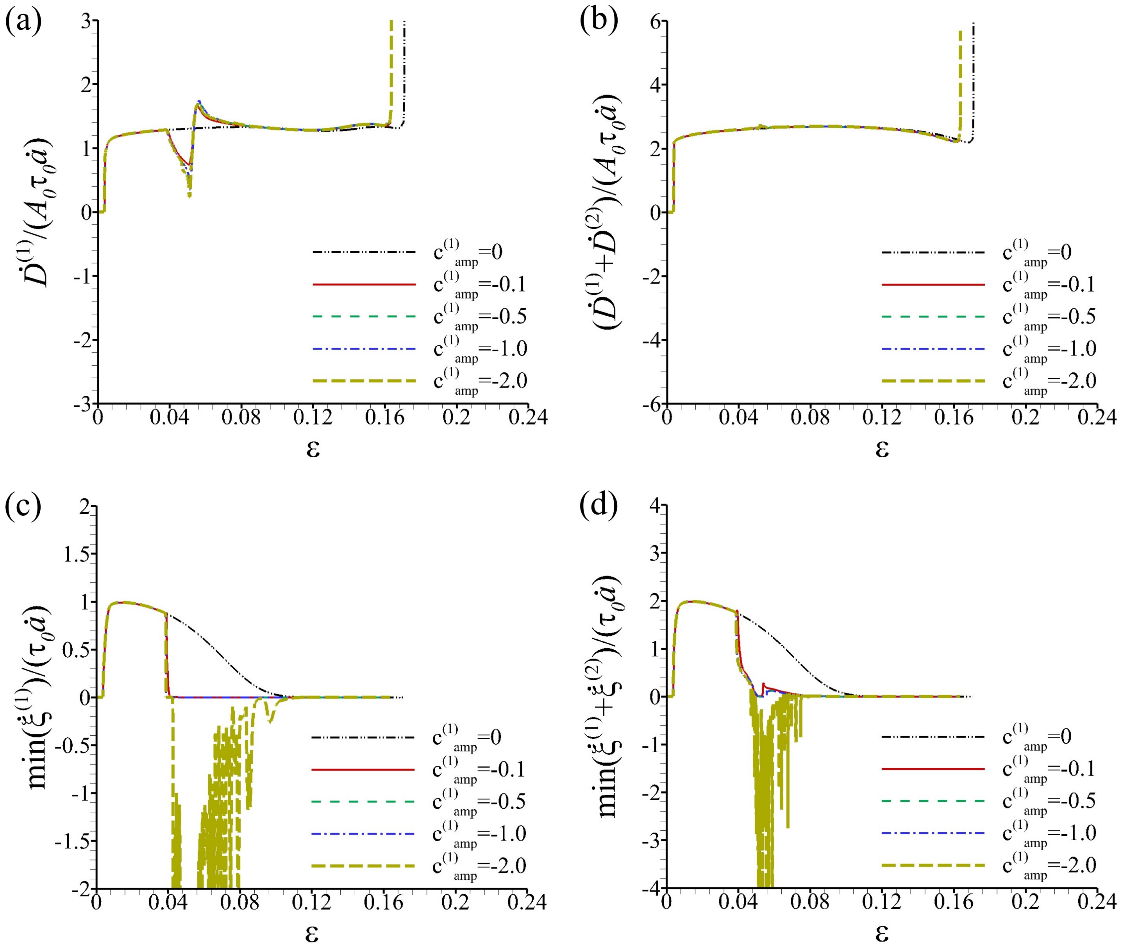

Figure 10: The variation of the normalized dissipation rate, $\dot{D}$, given by Eq. (30), with overall strain, ε, (a) for slip system (1) and (b) for slip systems (1) + (2). The variation of the minimum value of the normalized dissipation rate, $\min(\dot{\xi})$, at any point in the bar with ε (c) for slip system (1) and (d) for slip systems (1) + (2). The results are shown for cases with $\gamma_b^{(1)} = \gamma_b^{(2)} = 0.05$, $\gamma_e^{(1)} = \gamma_e^{(2)} = 0.02$, $p^{(1)} = p^{(2)} = 1$, $c_{\text{amp}}^{(2)} = 0$, and various values of $c_{\text{amp}}^{(1)}$.

where $\gamma_b^{(1)} = \gamma_b^{(2)} = 0.05$ and $\gamma_e^{(1)} = \gamma_e^{(2)} = 0.2$ so that the non-Schmid effect on the driving force for slip is active over a larger range of strain. The overall stress-strain responses for cases with $\gamma_b^{(1)} = \gamma_b^{(2)} = 0.05$, $\gamma_e^{(1)} = \gamma_e^{(2)} = 0.2$ and $c_{\text{amp}}^{(2)} = 0$ is shown in Fig. 4c. For sufficiently large values of $c_{\text{amp}}^{(1)}$ even the normalized values of $\dot{D}^{(1)}$ and $\dot{D}^{(1)} + \dot{D}^{(2)}$ can become strongly negative. Nevertheless, no instability is encountered prior to $\varepsilon = \varepsilon_f$. Although not shown here, the evolution of dissipation rate with ε for the calculations with $\gamma_b^{(1)} = \gamma_b^{(2)} = 0.05$, $\gamma_e^{(1)} = \gamma_e^{(2)} = 0.2$ and $c_{\text{amp}}^{(1)} = c_{\text{amp}}^{(2)}$ is similar to that in Fig. 12.

We now consider the response with a series of slip intervals over which non-Schmid governed slip occurs. Fig. 13 shows the overall stress-strain response for calculations with $\gamma_e^{(1)} = \gamma_e^{(2)} = 0.02$ and $p^{(1)} = p^{(2)} = 10$. In Fig. 13a, $\gamma_b^{(1)} = \gamma_b^{(2)} = 0$, while in Fig. 13c,

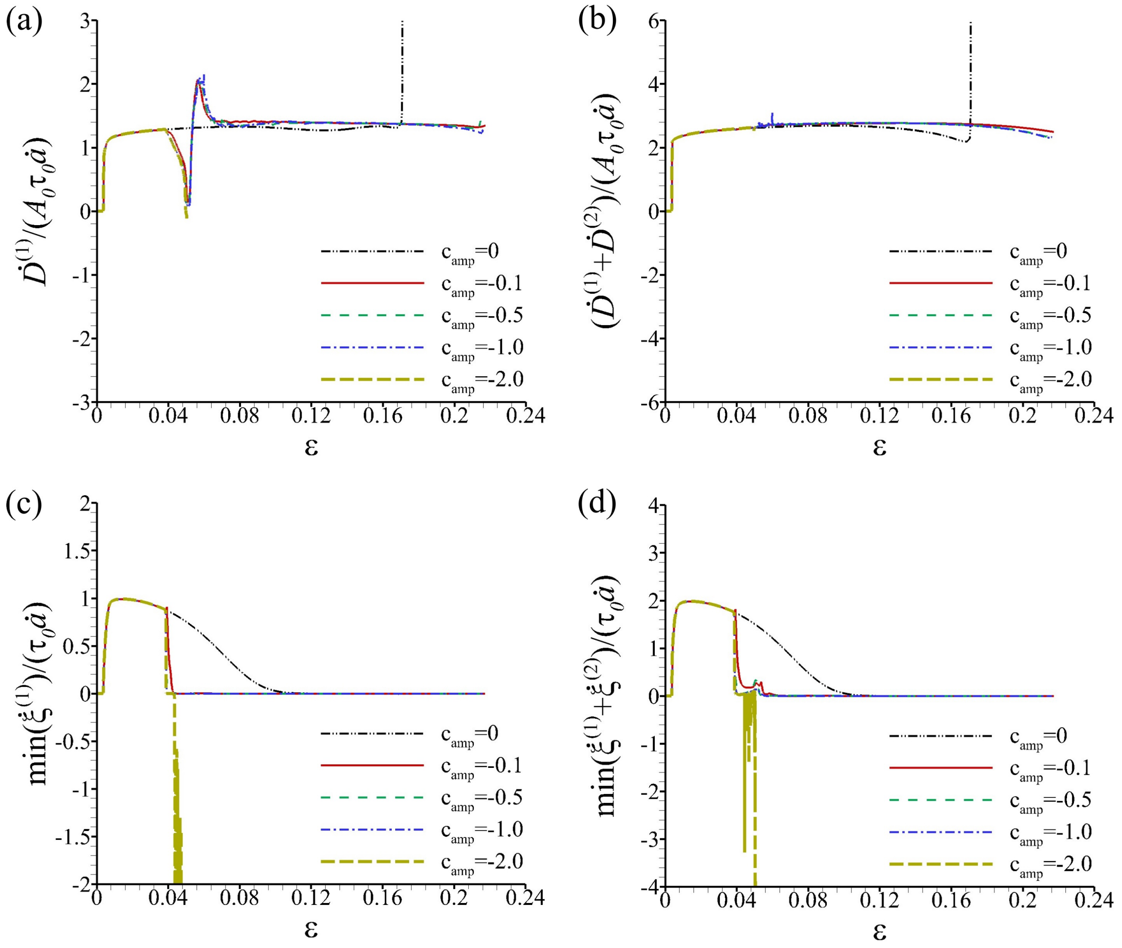

Figure 11: The variation of $\dot{D}$ with ε (a) for slip system (1) and (b) for slip systems $(1)+(2)$. The variation of $\min(\dot{\xi})$ with ε (c) for slip system (1) and (d) for slip systems $(1)+(2)$. The results are shown for cases with $\gamma_b^{(1)}=\gamma_b^{(2)}=0.05$, $\gamma_e^{(1)}=\gamma_e^{(2)}=0.02$, $p^{(1)}=p^{(2)}=1$, and various values of $c_{\rm amp}^{(1)}=c_{\rm amp}^{(2)}=c_{\rm amp}$.

$\gamma_b^{(1)}=\gamma_b^{(2)}=0.01$. In both figures, $c_{\rm amp}^{(2)}=0$, and the responses for various values of $c_{\rm amp}^{(1)}$ are shown. Similarly, in Fig. 13b, $\gamma_b^{(1)}=\gamma_b^{(2)}=0$, while in Fig. 13d, $\gamma_b^{(1)}=\gamma_b^{(2)}=0.01$, and the responses with various values of $c_{\rm amp}^{(1)}=c_{\rm amp}^{(2)}=c_{\rm amp}$ are shown.

In Figs. 13a and 13c, with $c_{\rm amp}^{(2)}=0$, the effect of the non-Schmid term on the overall stress-strain response is to increase the stress magnitude while it is active, but the effect nearly disappears thereafter. This does, however, lead to a decrease in the value ε_f. A comparison of these two figures shows that the effect of the value of γ_b, which dictates at what point in the deformation history the non-Schmid term becomes active, is not very strong on the overall stress-strain response due to the small difference in the values of $\gamma_b^{(\alpha)}$. Also, for nonuniform slip (i.e., for a bar with an initial geometric defect), the overall stress-strain response does not reflect the periodicity of $Z^{(\alpha)}$ in Eq. (27), as was the case for uniform

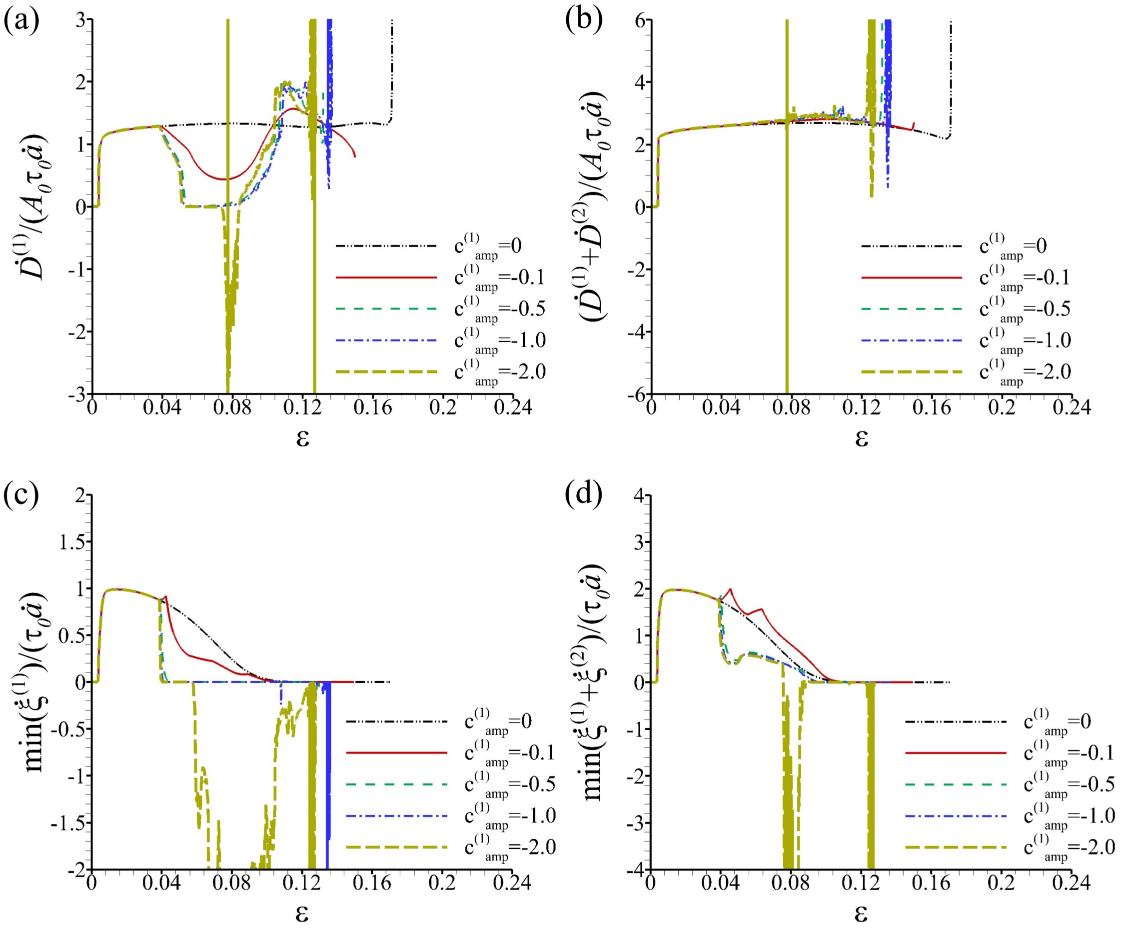

Figure 12: The variation of $\dot{D}$ with ε (a) for slip system (1) and (b) for slip systems $(1)+(2)$. The variation of $\min(\dot{\xi})$ with ε (c) for slip system (1) and (d) for slip systems $(1)+(2)$. The results are shown for cases with $\gamma_b^{(1)} = \gamma_b^{(2)} = 0.05$, $\gamma_e^{(1)} = \gamma_e^{(2)} = 0.2$, $p^{(1)} = p^{(2)} = 1$, $c^{(2)}_{\text{amp}} = 0$, and various values of $c^{(1)}_{\text{amp}}$.

slip shown in Fig. 2b. In Figs. 13b and 13d where $c^{(1)}_{\text{amp}} = c^{(2)}_{\text{amp}}$, very high stress magnitudes develop for $c_{\text{amp}} < -0.1$. Even though the overall stress magnitudes are higher, for both $c_{\text{amp}} = -0.1$ and $c_{\text{amp}} = -0.5$, the rapid drop in overall stress occurs at a smaller value of ε than for the comparison crystal with Schmid stress governed slip, $c_{\text{amp}} = 0$. For $c_{\text{amp}} \leq -1$, the overall stress-strain curves in both Figs. 13b and 13d initially follow the other curves for non-Schmid governed slip, but with a further increase in the value of the imposed strain ε, the stress tends to evolve almost linearly with strain, and the calculations terminate because the time step required for numerical stability becomes extremely small. With $c_{\text{amp}} \geq -0.5$ in Figs. 13b and 13d, the calculations are terminated following the rapid drop in overall stress.

The variation of the strain to failure, ε_f, with the amplitude of the non-Schmid term, $|c^{(1)}_{\text{amp}}|$ is shown in Fig. 14 for calculations with $p^{(1)} = p^{(2)} = 10$ for two cases; (i) $c^{(2)}_{\text{amp}} = 0$

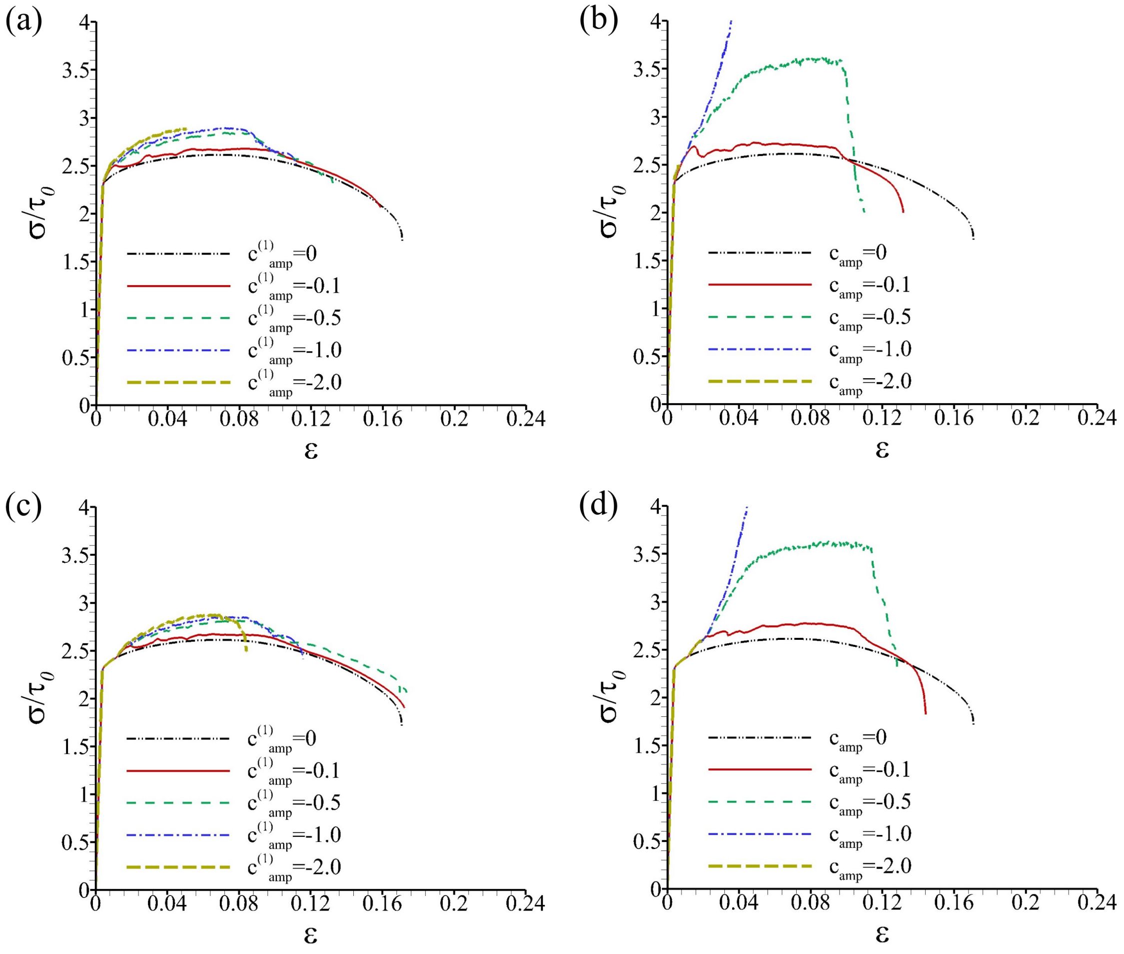

Figure 13: Overall stress-strain response for cases with (a) $\gamma_b^{(1)} = \gamma_b^{(2)} = 0$, $c_{\rm amp}^{(2)} = 0$, and various values of $c_{\rm amp}^{(1)}$; (b) $\gamma_b^{(1)} = \gamma_b^{(2)} = 0$, and various values of $c_{\rm amp}^{(1)} = c_{\rm amp}^{(2)} = c_{\rm amp}$; (c) $\gamma_b^{(1)} = \gamma_b^{(2)} = 0.01$, $c_{\rm amp}^{(2)} = 0$, and various values of $c_{\rm amp}^{(1)}$; and (d) $\gamma_b^{(1)} = \gamma_b^{(2)} = 0.01$, and various values of $c_{\rm amp}^{(1)} = c_{\rm amp}^{(2)} = c_{\rm amp}$. For all cases in (a)-(d), $\gamma_e^{(1)} = \gamma_e^{(2)} = 0.02$ and $p^{(1)} = p^{(2)} = 10$.

(Fig. 14a) and (ii) $|c_{\rm amp}^{(1)}| = |c_{\rm amp}^{(2)}|$ (Fig. 14b). The values of ε_f correspond to the overall strain at which the calculations terminate due to a rapid drop in overall stress, except for a few cases with larger magnitudes of $c_{\rm amp}$, where calculations are terminated because the time step required for numerical stability becomes extremely small even before the drop in overall stress. Results for $c_{\rm amp}^{(1)} = c_{\rm amp}$ (with $c_{\rm amp}^{(2)} = 0$) in Fig. 14a show that the variation of ε_f with $|c_{\rm amp}|$ is not necessarily monotonic. The results in Fig. 14b where $c_{\rm amp}^{(1)} = c_{\rm amp}^{(2)} = c_{\rm amp}$, show that for $\gamma_e < 0.05$, the value of ε_f decreases monotonically with increasing value of $|c_{\rm amp}|$, but for $\gamma_e = 0.05$, the dependence of ε_f on $|c_{\rm amp}|$ is non monotonic. Moreover, for $p^{(1)} = p^{(2)} = 10$ with $c_{\rm amp}^{(1)} = c_{\rm amp}$ and $c_{\rm amp}^{(2)} = 0$, the variation of ε_f with the value of γ_e is substantially greater than in Fig. 5a, where $p^{(1)} = p^{(2)} = 1$, while with $c_{\rm amp}^{(1)} = c_{\rm amp}^{(2)} = c_{\rm amp}$,

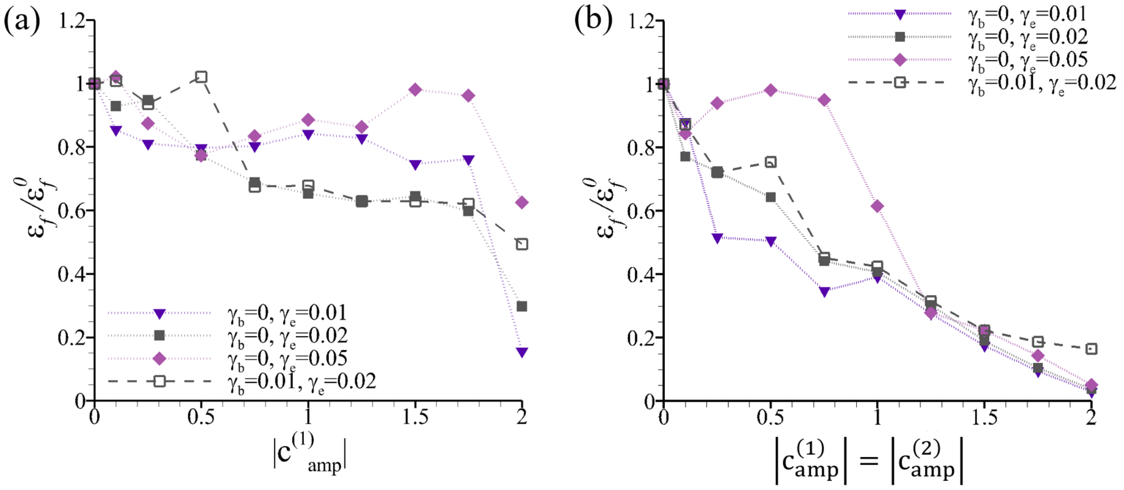

Figure 14: The variation of strain to failure, ε_f, with the magnitude of the non-Schmid parameter, (a) $c^{(1)}_{\rm amp}$ when $c^{(2)}_{\rm amp} = 0$, and (b) $c^{(1)}_{\rm amp} = c^{(2)}_{\rm amp} = c_{\rm amp}$, for various values of $\gamma_b^{(1)} = \gamma_b^{(2)} = \gamma_b$ and $\gamma_e^{(1)} = \gamma_e^{(2)} = \gamma_e$. For all cases in (a)-(b), $p^{(1)} = p^{(2)} = 10$ in Eq. (27). The normalization parameter ε_f^0 is the strain to failure for Schmid stress-governed slip.

the variation of ε_f with the value of γ_e is substantially smaller than in Fig. 5b, where $p^{(1)} = p^{(2)} = 1$.

Fig. 15 shows the variation of various measures of dissipation rate with overall strain, ε, for cases with $\gamma_b^{(1)} = \gamma_b^{(2)} = 0$, $\gamma_e^{(1)} = \gamma_e^{(2)} = 0.02$, $p^{(1)} = p^{(2)} = 10$ and $c^{(1)}_{\rm amp} = c^{(2)}_{\rm amp} = c_{\rm amp}$, for various values of $c_{\rm amp}$. The overall stress-strain responses are shown in Fig. 13b. The variation of the normalized dissipation rate $\dot{D}^{(1)}/(A_0\tau_0\dot{a})$ with ε is shown in Fig. 15a and the variation of the sum $(\dot{D}^{(1)} + \dot{D}^{((2)})/(A_0\tau_0\dot{a})$ is shown in Fig. 15b. Figs. 15c and 15d show the variations of the minimum values of $\dot{\xi}^{(1)}$ and of $\dot{\xi}^{(1)} + \dot{\xi}^{(2)}$, respectively. The values of $\dot{D}^{(1)}/(A_0\tau_0\dot{a})$ and $(\dot{D}^{(1)} + \dot{D}^{((2)})/(A_0\tau_0\dot{a})$ are negative for a small range of ε at an early stage of plastic deformation but both $\dot{D}^{(1)}/(A_0\tau_0\dot{a})$ and $(\dot{D}^{(1)} + \dot{D}^{((2)})/(A_0\tau_0\dot{a})$ remain positive during most of the strain interval where non-Schmid governed slip is active, although they oscillate wildly. Comparing Figs. 15c and 15d shows that at some stages of deformation, the value of $\dot{\xi}^{(2)}$ can be sufficiently positive so that even though $\dot{\xi}^{(1)}$ is negative, the sum $\dot{\xi}^{(1)} + \dot{\xi}^{(2)}$ is non-negative.

4. Concluding Remarks

Quasi-static plane strain tension of a planar single crystal with two potentially active slip systems, oriented for symmetric double slip, was analyzed for a rectangular bar with a small geometric imperfection to trigger nonuniform deformation. The crystal plasticity constitutive relation incorporates a non-Schmid stress into the expression for the driving force of the slip system shear rate. Calculations were carried out for crystals having non-Schmid stress affected slip on one or on both slip systems. In both cases, various characterizations

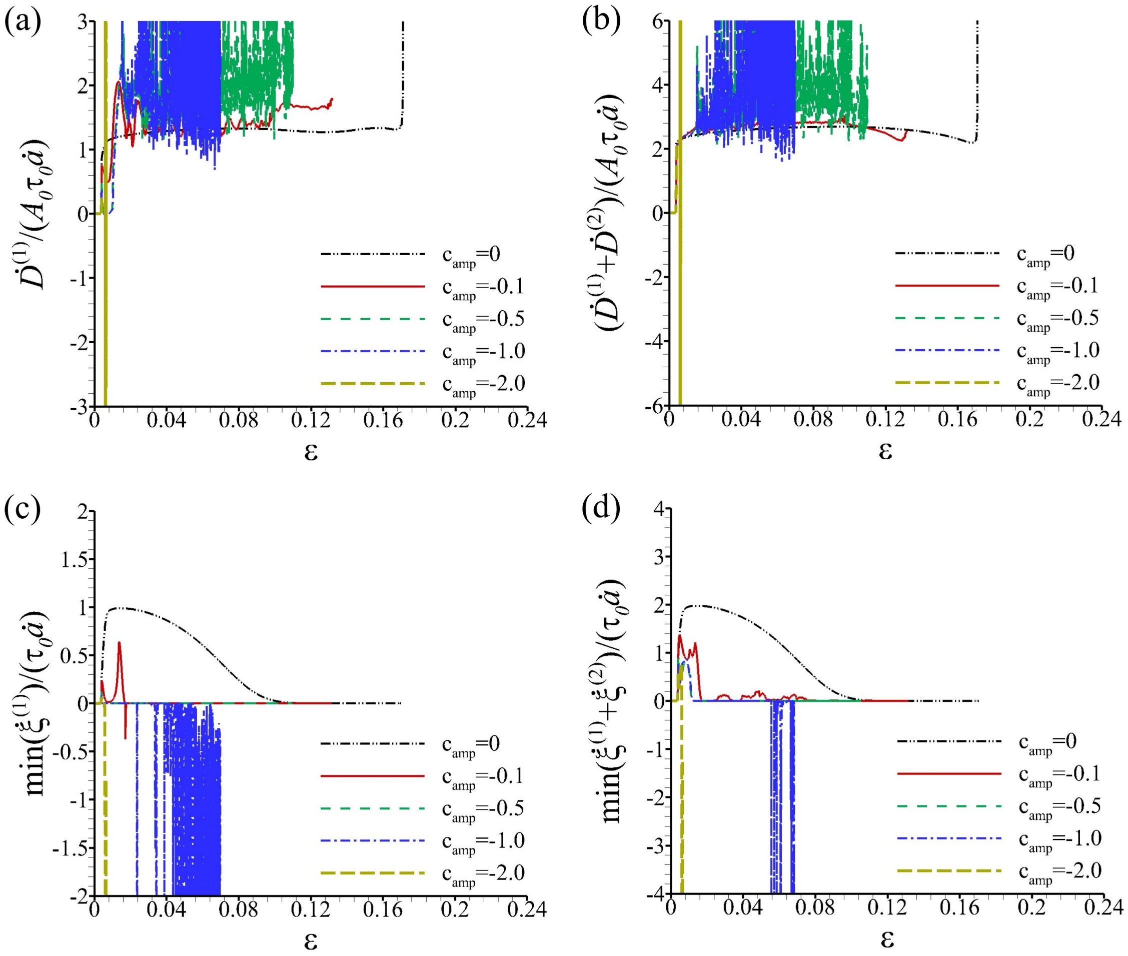

Figure 15: The variation of $\dot{D}$ with ε (a) for slip system (1) and (b) for slip systems (1) + (2). The variation of $\min(\dot{\xi})$ with ε (c) for slip system (1) and (d) for slip systems (1) + (2). The results are shown for cases with $\gamma_b^{(1)} = \gamma_b^{(2)} = 0$, $\gamma_e^{(1)} = \gamma_e^{(2)} = 0.02$, $p^{(1)} = p^{(2)} = 10$ in Eq. (27), and various values of $c_{\mathrm{amp}}^{(1)} = c_{\mathrm{amp}}^{(2)} = c_{\mathrm{amp}}$.

of the non-Schmid term were investigated. For comparison purposes, calculations were also carried out for a crystal with Schmid stress governed slip.

Results were presented for the effect of non-Schmid governed slip on the overall stress-strain response, on the strain at which a rapid drop in overall stress carrying capacity occurs, termed the failure strain, and on the evolution of the dissipation rate with the imposed straining. It was found that including a non-Schmid stress in the driving force expression can have a significant effect on the overall stress-strain response (Fig. 4) and on the slip mode that develops (Figs. 6 to 9). These effects can lead either to an increase or to a decrease in the failure strain (relative to that for Schmid stress governed slip), Figs. 5 and 14. All of these depend on: (i) whether non-Schmid governed slip is on one slip system or both slip systems; and (ii) the value of the parameters in Eqs. (26) and (27), the magnitude of the non-Schmid term ($c_{\mathrm{amp}}^{(\alpha)}$), the slip at which the non-Schmid term is active ($\gamma_b^{(\beta)}$), the slip interval over which the non-Schmid term is active ($\gamma_e^{(\beta)}$), and the number of non-Schmid slip events ($p^{(\beta)}$). Furthermore, the dependence of the failure strain on the parameters characterizing the non-Schmid dependence is not necessarily monotonic, Fig. 5.

In developing plastic constitutive relations, the requirement is generally imposed that the dissipation rate be non-negative at each point of the body analogous to the postulate of Coleman and Noll (1964) that requires the Clausius-Duhem inequality to be satisfied for all possible deformation histories. For a purely mechanical theory, i.e. temperature and entropy not included in the formulation (except possibly through material parameters depending on a temperature that has a rate proportional to the plastic dissipation rate), the requirement of a non-negative dissipation rate does not directly follow from the second law of thermodynamics. It is analogous to, but not derived from, the Clausius-Duhem inequality, e.g. Needleman (2024). In continuum slip crystal plasticity formulations, the even stronger requirement that the dissipation rate associated with each slip system is non-negative is generally imposed. This requirement is readily met when the slip on each system is only governed by the Schmid stress. When a non-Schmid stress is incorporated into the driving force, a non-negative dissipation rate is not guaranteed. The occurrence of a negative dissipation rate does not violate any fundamental physical principle. However, a physically based restriction on the magnitude or duration of a a non-positive dissipation rate may arise from consideration of the kinetics of plastic flow.

There are constitutive frameworks for which satisfaction of the Clausius-Duhem inequality can serve as a stability condition, Coleman and Mizel (1967); Dafermos (1979). In the quasi-static crystal plasticity calculations here, as in the one dimensional wave propagation problem of Needleman (2023), a negative dissipation rate with a sufficiently large magnitude occurring over a sufficiently long time can lead to an instability, either a physical instability or, depending on the parameters characterizing non-Schmid plasticity and/or the material strain rate sensitivity, a numerical instability. The present results for a quasi-static rate dependent continuum slip crystal plasticity problem, as those of Needleman (2023) for a one dimensional wave propagation problem, show that stable solutions can be obtained with a negative dissipation rate. Indeed, as seen in Fig. 12, stable solutions can be obtained even when the integrated dissipation rate is negative, $\sum_\alpha \dot{\mathcal{D}}^{(\alpha)}$, where $\dot{\mathcal{D}}^{(\alpha)}$ is given by Eq. (30). In addition, for plasticity theories with a nonassociative flow rule phenomena such as a flutter instability, Piccolroaz et al. (2006), and abrupt strain bursts can occur, Racherla and Bassani (2007); Bassani and Racherla (2011). The role, if any, of a negative dissipation rate in promoting such phenomena remains to be investigated.

The results here indicate that, quite generally, for rate dependent plastic constitutive relations imposing the requirement for the plastic dissipation rate to be non-negative at each point of the body for all times is overly restrictive. Presumably there is some condition that should be imposed to limit how negative the dissipation rate can be. Comparing Figs. 10 and 12 shows that if the slip range over which the pointwise dissipation rate is sufficiently small, the integrated dissipation rate $\dot{\mathcal{D}}$ remains non-negative. Imposing the requirement of a sufficiently short time interval or a sufficiently small slip interval over which a negative dissipation rate is allowed at some points of the body (based on the kinetics of plastic flow) would be qualitatively similar to the situation in statistical mechanics where, due to fluctuations, the Clausius-Duhem inequality is permitted to be violated over a sufficiently small distance for a sufficiently short time period. What is sufficiently small and what is sufficiently short remain to be delineated.

Acknowledgments

A.S. acknowledges the financial support provided by the U.S. National Science Foundation grant CMMI-1944496.

Appendix

For completeness, the derivation of the rate tangent expressions used in the calculations is briefly outlined. The derivation closely follows that for Schmid stress governed slip given by Peirce et al. (1983) and Needleman et al. (1985) where more detailed derivations are presented.

The slip increment on system (α) at time t is

$$\Delta\gamma^{(\alpha)} = \gamma^{(\alpha)}(t+\Delta t) - \gamma^{(\alpha)}(t) \tag{A-1}$$

Linear interpolation within the time increment gives

$$\Delta\gamma^{(\alpha)} = \left[(1-\theta)\dot{\gamma}^{(\alpha)}(t) + \theta\dot{\gamma}^{(\alpha)}(t+\Delta t)\right]\Delta t \tag{A-2}$$

Using a Taylor expansion for $\dot{\gamma}^{(\alpha)}(t+\Delta t)$

$$\dot{\gamma}^{(\alpha)}(t+\Delta t) = \dot{\gamma}^{(\alpha)}(t) + \frac{\partial\dot{\gamma}^{(\alpha)}}{\partial\chi^{(\alpha)}}\Delta\chi^{(\alpha)} + \frac{\partial\dot{\gamma}^{(\alpha)}}{\partial g^{(\alpha)}}\Delta g^{(\alpha)} + ... \tag{A-3}$$

Substituting Eq. (A-3) into Eq. (A-2) gives to first order

$$\Delta\gamma^{(\alpha)} = \dot{\gamma}_t^{(\alpha)} + (\theta\Delta t)\left[\frac{\partial\dot{\gamma}^{(\alpha)}}{\partial\chi^{(\alpha)}}\Delta\chi^{(\alpha)} + \frac{\partial\dot{\gamma}^{(\alpha)}}{\partial g^{(\alpha)}}\Delta g^{(\alpha)}\right] \tag{A-4}$$

where here and subsequently $(\ )_t$ denotes quantities evaluated at time t, e.g. $\dot{\gamma}_t^{(\alpha)} = \dot{\gamma}^{(\alpha)}(t)$.

Calculating the partial derivatives, using the definition of $\chi^{(\alpha)}$ in Eq. (12) and carrying out some algebraic manipulations analogous to those given by Peirce et al. (1983) and Needleman et al. (1985) leads to the equation to solve for $\Delta\gamma^{(\kappa)} = \dot{\gamma}^{(\kappa)}\Delta t$ as

$$\sum_{\kappa} N_{\alpha\kappa}\Delta\gamma^{(\kappa)} = \dot{\gamma}_t^{(\alpha)}\Delta t + \left(\frac{(\theta\Delta t)\dot{\gamma}_t^{(\alpha)}}{m}\right)\left[\frac{\bar{\mathbf{R}}^{(\alpha)} : \mathbf{D}}{\chi^{(\alpha)}}\right]\Delta t \tag{A-5}$$

with

$$\bar{\mathbf{R}}^{(\alpha)} = \sum_{\beta} c_{\alpha\beta}\mathbf{R}^{(\beta)} \tag{A-6}$$

where $\mathbf{R}^{(\beta)}$ is given by Eq. (7).

In Eq. (A-5)

$$N_{\alpha\kappa} = \delta_{\alpha\kappa} + \xi^{(\alpha)}\left[\frac{\bar{\mathbf{R}}^{(\alpha)} : \mathbf{P}^{(\kappa)}}{\chi^{(\alpha)}} + \mathrm{sign}(\chi^{(\kappa)})\frac{h_{\alpha\kappa}}{g^{(\alpha)}}\right] \tag{A-7}$$

and

$$\dot{\gamma}_t^{(\alpha)} = \dot{a}^{(\alpha)}\mathrm{sign}(\chi_t^{(\alpha)})\left[\left|\frac{\chi_t^{(\alpha)}}{g_t^{(\alpha)}}\right|\right]^{(1/m)} \tag{A-8}$$

Also,

$$\xi^{(\alpha)} = \left(\frac{\theta\Delta t\dot{\gamma}_t^{(\alpha)}}{m}\right) \tag{A-9}$$

Define

$$\mathbf{Q}^{(\alpha)} = \xi^{(\alpha)}\left[\frac{\bar{\mathbf{R}}^{(\alpha)}}{\chi^{(\alpha)}}\right] \tag{A-10}$$

Using the notation of Peirce et al. (1983)

$$\dot{f}^{(\kappa)} = \sum_{\delta} N_{\kappa\delta}^{-1}\dot{\gamma}_t^{(\delta)} \qquad \mathbf{F}^{(\kappa)} = \sum_{\delta} N_{\kappa\delta}^{-1}\mathbf{Q}^{(\delta)} \tag{A-11}$$

Eq. (A-5) then gives

$$\frac{\Delta\gamma^{(\alpha)}}{\Delta t} = \dot{f}^{(\alpha)} + \mathbf{F}^{(\alpha)} : \mathbf{D} \tag{A-12}$$

and substituting $\Delta\gamma^{(\alpha)}/\Delta t$ for $\dot{\gamma}^{(\alpha)}$ in Eq. (7) results in the rate tangent expression

$$\dot{\boldsymbol{\tau}}^c = \mathbf{L}^{\tan} : \mathbf{D} - \sum_{\alpha} \dot{f}^{(\alpha)}\mathbf{R}^{(\alpha)} - \mathbf{D}\cdot\boldsymbol{\tau} - \boldsymbol{\tau}\cdot\mathbf{D} \tag{A-13}$$

where

$$\mathbf{L}^{\tan} = \left(\mathbf{L} - \sum_{\alpha}\mathbf{F}^{(\alpha)} : \mathbf{R}^{(\alpha)}\right) \tag{A-14}$$

The rate tangent expressions are the same as those given by Peirce et al. (1983) and-Needleman et al. (1985) but with $\chi^{(\alpha)}$ replacing $\tau^{(\alpha)}$ and $\bar{\mathbf{R}}^{(\alpha)}$ replacing $\mathbf{R}^{(\alpha)}$ in the expression for $\mathbf{Q}^{(\alpha)}$.

The rate independent limit corresponds to $m \to 0$ with $\Delta t > 0$ so that $\xi^{(\alpha)} \to \infty$. In that limit, $\dot{f}^{(\alpha)} = 0$, $\mathbf{F}^{(\alpha)}$ is independent of $\xi^{(\alpha)}$ and $N_{\kappa\delta}^{-1}$ is replaced by the inverse of the expression in [.] in Eq. (A-7).

References

Asim, U.B., Zhan, Z., Radovic, M. and Srivastava, A., 2022. Modeling the non-Schmid crystallographic slip in MAX phases. International Journal of Plasticity, 157, p.103399.

Bassani, J. L., Racherla, V., 2011. From non-planar dislocation cores to non-associated plasticity and strain bursts. Prog.Mat. Sci. 56.852-863.

Cereceda, D., Diehl, M., Roters, F., Raabe, D., Perlado, J.M. and Marian, J., 2016. Unraveling the temperature dependence of the yield strength in single-crystal tungsten using atomistically-informed crystal plasticity calculations. Int. J. Plast. 78, 242-265.

Chaussidon, J., Robertson, C., Rodney, D., Fivel, M., 2008. Dislocation dynamics simulations of plasticity in Fe laths at low temperature. Acta Mater. 56, 5466-5476.

Chen, P., Ghassemi-Armaki, H., Kumar, S., Bower, A., Bhat, S., Sadagopan, S., 2014. Microscale-calibrated modeling of the deformation response of dual-phase steels. Acta. Mater. 65, 133–149.

Coleman, B., Mizel, V.J., 1967. Existence of entropy as a consequence of asymptotic stability. Arch. Rat. Mech. Analysis, 25, 243-270.

Coleman, B.D., Noll, W., 1964. The thermodynamics of elastic materials with heat conduction and viscosity. Arch. Ration. Mech. Anal. 13, 167–178.

Dafermos, C.M., 1979. The second law of thermodynamics and stability. Arch. Rat. Mech. Analysis 70, 167-179.

Evans, D.J., Searle, D.J., 2002. The fluctuation theorem. Adv. Phys. 51, 1529-1585.

Ghorbanpour, S., Alam, M.E., Ferreri, N.C., Kumar, A., McWilliams, B.A., Vogel, S.C., Bicknell, J., Beyerlein, I.J. and Knezevic, M., 2020. Experimental characterization and crystal plasticity modeling of anisotropy, tension-compression asymmetry, and texture evolution of additively manufactured Inconel 718 at room and elevated temperatures. Int. J. Plast. 125, 63-79.

Ghorbanpour, S., Zecevic, M., Kumar, A., Jahedi, M., Bicknell, J., Jorgensen, L., Beyerlein, I.J. and Knezevic, M., 2017. A crystal plasticity model incorporating the effects of precipitates in superalloys: application to tensile, compressive, and cyclic deformation of Inconel 718. Int. J. Plast. 99, 162-185.

Gröger, R., 2021. Symmetry-adapted single crystal yield criterion for non-Schmid materials.Int. J. Plast. 146, 103101.

Gröger, R., Bailey, A.G. and Vitek, V., 2008. Multiscale modeling of plastic deformation of molybdenum and tungsten: I. Atomistic studies of the core structure and glide of 1/2¡ 1 1 1¿ screw dislocations at 0K. Acta Mater. 56, 5401-5411.

Gröger, R., Racherla, V., Bassani, J.L. and Vitek, V., 2008. Multiscale modeling of plastic deformation of molybdenum and tungsten: II. Yield criterion for single crystals based on atomistic studies of glide of 1/2¡ 111¿ screw dislocations. Acta Mater. 56, 5412-5425.

Gröger, R. and Vitek, V., 2020. Single crystal yield criterion for chromium based on atomistic studies of isolated 1/2 [111] screw dislocations. Int. J. Plast. 132, 102733.

Hussein, A.M., Rao, S.I., Michael Uchic, D., Dimiduk, D.M., El-Awady, J.A., 2015. Microstructurally based cross-slip mechanisms and their effects on dislocation microstructure evolution in fcc crystals. Acta Mater. 85, 180–190.

Jarzynski, C., 2010. Equalities and inequalities: irreversibility and the second law of thermodynamics at the nanoscale. Séminaire Poincaré XV Le Temps, 77–102.

Knezevic, M., Beyerlein, I.J., Lovato, M.L., Tomé, C.N., Richards, A.W. and McCabe, R.J., 2014. A strain-rate and temperature dependent constitutive model for BCC metals incorporating non-Schmid effects: Application to tantalum–tungsten alloys. Int. J. Plast. 62, 93-104.

Koester, A., Ma, A. and Hartmaier, A., 2012. Atomistically informed crystal plasticity model for body-centered cubic iron. Acta Mater. 60, 3894-3901.

Lim, H., Weinberger, C.R., Battaile, C.C. and Buchheit, T.E., 2013. Application of generalized non-Schmid yield law to low-temperature plasticity in bcc transition metals. Modelling and Simulation in Materials Science and Engineering, 21(4), p.045015.

Lim, H., Hale, L.M., Zimmerman, J.A., Battaile, C.C. and Weinberger, C.R., 2015. A multi-scale model of dislocation plasticity in α-Fe: Incorporating temperature, strain rate and non-Schmid effects. International Journal of Plasticity, 73, pp.100-118.

Malka-Markovitz, A., Devincre, B., Mordehai, D., 2021. A molecular dynamics-informed probabilistic cross-slip model in discrete dislocation dynamics. Scripta Mater. 190, 7–11.

Needleman, A., 1988. Material rate dependence and mesh sensitivity in localization problems. Comput. Methods Appl. Mech. Eng. 67, 69-85.

Needleman, A., 2023. Discrete defect plasticity and implications for dissipation. Eur. J. Mech./A Solids 100, 105002.

Needleman, A., 2024. A perspective on plasticity, dissipation and the second law of thermodynamics. ASME

J. Appl. Mech. 91, 061003.

Needleman, A., Asaro, R. J., LeMonds, J., Peirce, D., 1985 Finite element analysis of crystalline solids. Comp. Meth. Appl. Mech. Engin. 52, 689-708.

Ostoja-Starzewski, M., Laudani, R., 2020. Violations of the Clausius–Duhem inequality in Couette flows of granular media. Proc. R. Soc. A476, 20200207.

Patra, A., Zhu, T. and McDowell, D.L., 2014. Constitutive equations for modeling non-Schmid effects in single crystal bcc-Fe at low and ambient temperatures. Int. J. Plast., 59, 1-14.

Peirce, D., Asaro, R.J. and Needleman, A., 1983. Material rate dependence and localized deformation in crystalline solids. Acta Metall. 31, 1951-1976.

Piccolroaz, A., Bigoni, D., Willis, J. R., 2006. A dynamical interpretation of flutter instability in a continuous medium. J. Mech. Phys. Solids 54, 2391-2417.

Qin, Q., Bassani, J.L., 1992. Non-Schmid yield behavior in single crystals. J. Mech. Phys. Solids 40, 813-833.

Racherla, V., Bassani, J. L., 2007. Strain burst phenomena in the necking of a sheet that deforms by non-associated plastic flow. Modelling Simul. Mater. Sci. Eng. 15, S297-S311.

Ranjan D., Narayanan S., Kadau K., Patra1 A., 2021. Crystal plasticity modeling of non-Schmid yield behavior: from Ni_3Al single crystals to Ni-based superalloys Modelling Simul. Mater. Sci. Eng. 29, 055005.

Srivastava, A., Ghassemi-Armaki, H., Sung, H., Chen, P. Kumar, S., Bower, A.F., 2015. Micromechanics of plastic deformation and phase transformation in a three-phase TRIP-assisted advanced high strength steel: Experiments and modeling. J. Mech. Phys. Solids 78, 46-69.

Vitek, V., Mrovec, M., Bassani, J.L., 2004. Influence of non-glide stresses on plastic flow: from atomistic to continuum modeling. Mat. Sci. Engg. A365, 31-37.

Vitek, V., Paidar, V., 2008. Non-planar dislocation cores: a ubiquitous phenomenon affecting mechanical properties of crystalline materials. in: Dislocations in Solids,ed. J.P. Hirth, Ch. 87, Elsevier, Amsterdam.

Wang, Z.Q., Beyerlein, I.J., 2011. An atomistically-informed dislocation dynamics model for the plastic anisotropy and tension–compression asymmetry of BCC metals. Int. J. Plast. 27, 1471-1484.

Wang, G.M., Sevick, E.M., Mittag, E., Searles, D.J., Evans, D.J., 2010. Experimental demonstration of violations of the second law of thermodynamics for small systems and short time scales. Phys. Rev. Letts. 89, 050601.

Weinberger, C.R., Battaile, C.C., Buchheit, T.E., Holm, E.A., 2012. Incorporating atomistic data of lattice friction into BCC crystal plasticity models. Int. J. Plast. 37, 16–30.

Zhan, Z., Chen, Y., Radovic, M. and Srivastava, A., 2020. Non-classical crystallographic slip in a ternary carbide–Ti2AlC. Mat. Res. Letts 8, 275-281.

Zhan, Z., Radovic, M. and Srivastava, A., 2021. On the non-classical crystallographic slip in Tin+ 1AlCn MAX phases. Scripta Mater. 194, 113698.